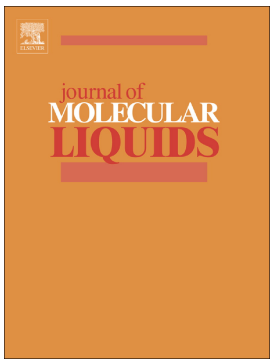

Molecular insights into inclusion complex formation between β- and γ-cyclodextrins and rosmarinic acid

F. Fateminasab, A.K. Bordbar, S. Shityakov, A.A. Saboury

PII: S0167-7322(20)32906-8

DOI: https://doi.org/10.1016/j.molliq.2020.113802

Reference: MOLLIQ 113802

To appear in: *Journal of Molecular Liquids*

Received date: 6 May 2020

Revised date: 29 June 2020

Accepted date: 10 July 2020

Please cite this article as: F. Fateminasab, A.K. Bordbar, S. Shityakov, et al., Molecular insights into inclusion complex formation between β- and γ-cyclodextrins and rosmarinic acid, *Journal of Molecular Liquids* (2018), https://doi.org/10.1016/j.molliq.2020.113802

Molecular insights into inclusion complex formation between β- and γ-cyclodextrins and rosmarinic acid

F. Fateminasab[a], A. K. Bordbar[a,b*]. S. Shityakov[c], A. A. Saboury[d*]

[a]Department of Chemistry, University of Isfahan, Isfahan, 8174673441, Iran

[b]California Institute for Quantitative Biosciences (QB3), University of California, Berkeley, California 94720, USA

[c]Department of Bioinformatics, University of Würzburg, 97074, Würzburg, Germany

[d]Institute of Biochemistry and Biophysics, University of Tehran, Tehran, Iran

[*]To whom correspondence should be addressed

[b] Emails: akbordbar@berkeley.edu and akbordbar@gmail.com
Tel: +1 (408) 594 6952

[d] Email: saboury@ut.ac.ir

Tel: +98-21-66956984

Abstract

In this study, we have investigated the stable inclusion complexes (IC) formation between β- and γ-cyclodextrin (γ-CyD) with rosmarinic acid (RA), a substance known to have antioxidant and anti-inflammatory effects. The β- and γ-CyD: RA ICs were prepared and characterized using experimental (^{1}H-NMR, FTIR, ICD and XRD, SEM) and computational techniques, such as molecular dynamics simulations and molecular docking. The thermodynamic parameter analysis showed that the formation of these ICs with the 1:1 molar ratio (A_L type) and also, the apparent stability constant (K_C) for β- and γ-CyD: RA ICs at 25 °C, were 79.07 ± 13.84 and 63.62 ± 9.31 L mol^{-1} respectively. Moreover, these results indicated that the encapsulation RA into the cavity of β- and γ-CyD: RA are exothermic ($\Delta H^0 < 0$) driven by the hydrophobic force and H-bond formations. Additionally, the experimental and theoretical methods confirmed that the β-CyD: RA IC is more stable than γ-CyD: RA IC. The computational results also confirm the formation of two stable IC. These results indicated that β- and γ-CyDs are promising excipients to formulate different substances, including RA to potentiate its antioxidant and anti-inflammatory activity bioavailability, solubility, and stability.

Keywords: β-cyclodextrin; γ-cyclodextrin; molecular dynamics simulations; rosmarinic acid; antioxidant; photo-stability.

Abbreviations

Antioxidant activity	AC
2,2'-azino-bis-3-ethylbenzothiazoline-6-sulphonic acid	ABTS
Beta-cyclodextrin	β-CyD
Rosmarinic acid	RA
scanning electron microscopy	SEM
Fourier-transform infrared spectroscopy	FT-IR
Gamma-cyclodextrin	γ-CyD
6-hydroxy-2, 5, 7, 8-tetramethychroman- 2-carboxylic acid	Trolox
Molecular dynamics	MD
Molecular mechanics generalized Born surface area	MM-GBSA
Molecular mechanics Poisson–Boltzmann surface area	MM-PBSA
The powder X-ray diffraction	PXRD
Root mean square displacement	RMSD
Radial distribution function	RDF
Hydrogen nuclear magnetic resonance spectroscopy	^{1}HNMR
solvent accessible surface area	SASA
Buried surface area	BSA
Center of mass	CoM

Introduction

Phenolic acids are the group of low molecular weight polyphenols, also known as plant secondary metabolites that can be divided into benzoic acid and cinnamic acid derivatives [1]. These compounds are believed to be quite effective at neutralizing free radicals [2]. They also include rosmarinic acid (RA), which is a caffeic acid ester of 3-(3,4-dihydroxyphenyl)lactic acid found in some plants, such as rosemary, basil, oregano and sage [3–5]. It has a variety of activities biological, containing antioxidant [6], anti-inflammatory, anticancer, antiviral, antimicrobial, properties, and neuroprotective effect [5,7–9]. The improvements in RA solubility and stability can be achieved via its efficient complexation with hydrophilic cyclodextrins (CyDs), which are broadly used in the pharmaceutical industry [10].

CyDs are composed of the units of α-1, 4-linked cyclic oligosaccharides of D-glucopyranose forming a doughnut-like molecule. CyDs can be applied in the pharmaceutical, food, cosmetic, and textile industries [11–15]. In particular, β-CyD is most widely used for pharmaceutical applications due to its low price, safety, biocompatibility, suitable cavity size, and efficient drug loading [16]. On the other hand, γ-CyD has a larger central cavity, which is more flexible and non-coplanar, increasing its solubility [16,17].

The native, unmodified CyDs are named α-CyD (6 units), β-CyD (7 units), and γ-CyD (8 units) [11,18] and forming the hydrophobic central cavity and the hydrophilic outer surface (Del Valle, 2004). As the host molecules, CyDs can form inclusion complexes (IC) with several hydrophobic guest compounds [11,18–20]. The insertion of "guest" molecules, such as drugs, vitamins, or food ingredients into the CyD cavity of CyDs, is mediated by the release of water molecules from this cavity [11,21].

Some CyDs has already been investigated to form ICs with antioxidant molecules, such as RA [19,21]. Some investigations have studied the formation of ICs of modified and unmodified CyDs with RA by CUPRAC (CUPric Reducing Antioxidant Capacity) methodology at the presence of modified and unmodified CyDs in the aqueous environment [3]. Moreover, the formation of β-CyD/RA IC has been explored by Medronho and *et al.* (2014) to determine its stoichiometry by ^{1}H-NMR titration [8]. Additionally, the RA antioxidant effects were measured in the presence of β-CyD to showing an increase in scavenging free radicals from the cells [8]. Therefore, this study aims to confirm the previous results and to provide new molecular insights into inclusion complex formation between native cyclodextrins and rosmarinic acid

characterizing this IC and analyzing its phase solubility, thermodynamic properties, photo-stability to improve the antioxidant and other bioactive effects of RA (Scheme 1).

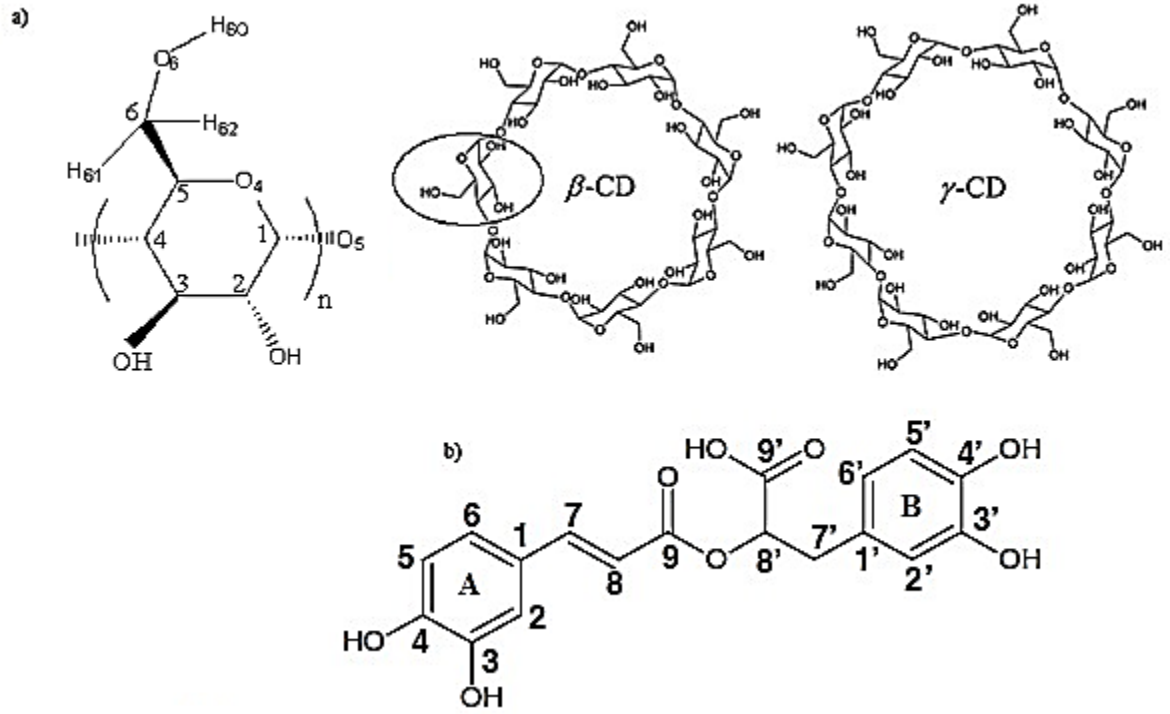

Scheme (1): The molecular structure of a) CyDs (n=7, β-CyD and n=8 γ-CyD) and b) RA

2. Materials and methods

2.1. Materials

β- and γ-CyD (>98 %), RA (>96 %), 6-hydroxy-2,5,7,8-tetramethylchroman-2-carboxylic acid (Trolox) (>97%), potassium persulfate, 2, 2′-azinobis (3-ethylbenzothiazoline-6-sulfonic acid) (ABTS) (>98%,) and methanol were obtained from Sigma-Aldrich (UK). The high-purity solvent (D_2O) was purchased from Merck Company (Germany). Ultrapure water (17.0 MΩ/cm resistivity; Nano pure infinity, Barnstead, USA) was applied for preparing phosphate buffer (PBS, 10 mmol L^{-1}, pH 7.4).

2.2. Preparation of (β- and γ-) CyDs: RA IC

To prepare the (β- and γ-) CyDs: RA ICs formation, according to the values listed in Table 1, (β- and γ-) CyDs were dissolved in 12 mL deoxygenized ultrapure water (by blowing of N_2 gas for

15 minutes) and RA (more than 1 to 1 molar ratio) dissolved in methanol in glass capped vials. Next, stirred in neutral pH for one day to achieve the thermodynamic equilibrium at ambient temperature. Ultimately, the mixture of CyDs and RA was centrifuged (10000 rpm, 10 min), and then the supernatant of the mixture of CyDs and RA (VaCo5, Zirbus, Germany; 1.30×10^{-1} mBar and -50 °C). These powder of IC were stored at -4 °C [21,22].

Table 1. The required values for the preparation of ((β- and γ-) CyDs: RA IC

Host	Weight (g)	Guest	Weight (g)	Solvent of RA
β-CyD	0.200	RA	0.070	methanol
γ-CyD	0.200	RA	0.060	methanol

2.3. Phase solubility analysis

The studies of phase solubility were performed for (β- and γ-) CyDs: RA IC by Higuchi and Connors technique [23]. Firstly, 1900 μL of various concentration of CyDs (0, 0.475, 0.95, 1.90, 2.85, 3.80, and 4.75 μmol L^{-1}) were provided by the deoxygenized PBS (pH 7.4, 10 mmol L^{-1}) and then mixed with 100 μL RA dissolved in methanol (10 mmol L^{-1}). These solutions were added to the *seal foil coating* vials to prevent photo-degradation, evaporation, and oxidation. Besides, vials were sited in Cooling Shaker Incubator (Jal Tajhiz, JTSDL40, and Iran) for three days at 15, 18, 21, and 25 °C, to equilibrate the complexation. Afterward, the mixtures were cleared by using the 0.45 μm millipore membrane filter, and the RA concentration was determined spectrophotometrically at 324 nm in the supernatant by a UV/Vis Spectrophotometer, equipped with a thermostat (Perkin Elmer, Lambda 265, USA) [24].

The apparent stability constant (K_C) for the ICs were evaluated from the phase solubility analysis along with the following equation (1) [11,25]:

$$K_C = \frac{slope}{S_0(1 - slope)} \qquad (1)$$

Where S_0 (y-intercept) is the intrinsic solubility of RA in the water in the absence of CyDs.

The binding analysis was applied at 15, 18, 21, and 25 °C. The $\Delta G^{\circ\prime}$ of binding (kJ mol^{-1}), was achieved by the following equation (2):

$$\Delta G^{0\prime} = -RTln(K_C/\mathrm{L\ mol^{-1}}) \qquad (2)$$

The thermodynamic parameters (*ΔG°′, ΔH°′,* and *ΔS°′*) were measured by the following equation (3):

$$\ln(K_C/\text{L mol}^{-1}) = -\frac{\Delta H^{0\prime}}{RT} + \frac{\Delta S^{0\prime}}{R} \qquad (3)$$

Where *ΔH°′, ΔS°′, ΔG°′,* [26] T, and R are the standard enthalpy change (kJ mol^{-1}), the standard entropy change (J mol^{-1}), the standard Gibbs free energy change (kJ mol^{-1}), absolute temperature (K) and gas constant (J mol^{-1} K^{-1}) in that order.

2.4. The characterization of (β- and γ-) CyDs: RA IC

The Fourier-transform infrared spectra (FT-IR) of pure RA, (β- and γ-) CyDs, and (β- and γ-) CyDs: RA IC, were recorded at ambient temperature in the 4000–400 cm^{-1} wavenumber range (with 4 cm^{-1} resolution) with the FT-IR spectrometer (JASCO, FT/IR-6300, Japan). These compounds were organized on a KBr pellet in vacuum desiccators under a 0.01 torr pressure.

Hydrogen nuclear magnetic resonance spectroscopy (^{1}H-NMR) for pure RA, (β- and γ-) CyDs and the IC of (β- and γ-) CyDs: RA was accomplished in D_2O at 25 ˚C in 0 to 12 ppm range using Spectrometer of ^{1}H-NMR (Varian-INOVA 500 MHz, USA). The observed sharp signal around 4.76 ppm is in regards to HDO that produced as a result of the exchange of protons between (β- and γ-) CyDs and also O-H (phenolic and acidic) in RA with D_2O. The resonance of HDO, as the lock frequency, set to 4.76 ppm to receive the uniform of values for the chemical shifts. The change of chemical shift calculation (Δδ) was achieved along with the following equation (4):

$$\Delta\delta = \delta_{complex} - \delta_{free} \qquad (4)$$

Where δ_{free} and $\delta_{complex}$ are the chemical shifts of pure compounds (RA and (β- and γ-) CyDs) and β- and γ-) CyDs: ICs, respectively.

The scanning electron microscope (SEM) demonstrated micrographs of RA, (β- and γ-) CyDs, and ICs were used (Zeiss, Sigma, VP-500 EDS, and Germany) at an acceleration voltage of 15 kV. A thin gold layer coated these compounds in a vacuum.

Another method for the characterization of IC is X-ray diffraction (XRD) that commonly applied to probe the hosts (CyDs), guests (drugs), and their ICs crystals structure. The diffraction patterns of XRD for (β- and γ-) CyDs, RA, and IC of (β- and γ-) CyDs: Cu-X-Ray Tube Anode

measured RA, Cu, Ni-filtered, Cu Kα radiation wavelength = 1.541874 Å and a 40 kV voltage, 35 mA current density and in an angle of diffraction (2θ) range of 5-100 ° at 0.05 ° min^{-1} rate achieved with an X-ray diffractometer (Rigaku Ultima IV XRD, Japan). These compound powders were packed a rectangular aluminum cell and finally exposed to the beam of X-ray.

The spectra of Induced Circular Dichroism (ICD) for RA, (β- and γ-) CyDs, and IC of (β- and γ) CyDs: RA (0.5 mg mL^{-1}) were achieved in a PBS (pH 7.4, 10 mmol L^{-1}) on a CD Spectrophotometer (Aviv, Model-215, USA). A 0.1 cm-thick quartz cell was applied in the region of near-UV (250 to 350 nm) at ambient temperature.

2.5. Encapsulation efficiency and loading capacity

In order to obtain the encapsulation efficiency (EE%) and loading capacity (LC%) of the RA in the cavity of CyDs (β- and γ-), 5 mL of 1 mg mL^{-1} solution of ICs was stirred at room temperature for one day. The samples were then centrifuged for 5 min at 10000 rpm, and the concentrations of the RA were calculated using a spectrophotometer UV-vis during the wavelength of 324 nm that was the maximum absorbance. All measurements were performed three times in the same condition. The values of LC% and EE% of the desired complexes and pure host and guests were determined using the following two equations:

$$LC(\%) = \frac{RA_{\exp}(\mathrm{mg})}{IC(\mathrm{mg})} \times 100 \qquad (5)$$

$$EE\% = \frac{RA_{\exp}(\mathrm{mg})}{RA_T(\mathrm{mg})} \times 100 \qquad (6)$$

Where, RA_{exp} and RA_T denote the entrapped amount of RA and the initial quantity of RA, respectively.

2.6. Photo-stability

The photo-stability studies of the pure RA (50 μmol L^{-1}) and complexed RA (1 mg mL^{-1}) in aqueous solution was investigated using two UVC lamps (254 nm, 8 W). At first, the solutions of RA in free and complexed states with appropriate concentration were prepared and dehydrogenated. Examining the photo-stability under the UVC lamp, the sample solution was irradiated in a quartz cuvette and stirred for a specified time. The concentration of the

decomposed guest compound can be measured by assessing the absorbance at 324 nm by spectrophotometer of UV/Vis at a given time of 0, 20, 40, 60, 80, 100 and 120 min [27].

2.7. Antioxidant activity

This antioxidant activity study was accomplished to evaluate and compare the RA antioxidant activity in pure and complexed states with (β- and γ-) CyDs. These experiments were performed according to the following steps:

- Preparation of solutions with different concentrations and molar ratios of CyD and drug form 30, 45, 60, 75, and 90 μmol L^{-1} and different molar ratios of β- and γ-CyDs: RA in 1:1, 1:1.5, 1:2, 1:2.5 and 1:3.
- Producing of ABTS radical cation ($ABTS^{\bullet+}$), the ABTS stock solution (10 mL, 7 mmol L^{-1}) was prepared in water and added potassium persulfate solution (1.1 mL, 24.5 mmol L^{-1}) and then to allow free radical generation, this solution covered with foil and placed in the dark for 14–16 hours. Finally, the $ABTS^{\bullet+}$ solution was diluted by PBS to reach specific absorbance value of 0.65-0.75 at 734 nm.
- Preparation of 1 mmol L^{-1} standard solution of Trolox.
- To evaluate of scavenging effect of the antioxidant samples, 900 μL of $ABTS^{\bullet+}$ solution added to 100 μL of the sample solutions with different concentrations and molar ratios of (β- and γ)-CyDs and RA. and then to record the UV/vis absorption at 734 nm after 10 min incubation.
- Determination of the samples antioxidant activity as inhibition percent of $ABTS^{\bullet+}$ via the following equation:

$$ABTS^{\bullet+}\ Inhibition(\%) = (1 - \frac{A_S}{A_C}) \times 100 \qquad (7)$$

Where A_S and A_C are the absorptions of $ABTS^{\bullet+}$ in the presence and absence of sample, in that order.

2.8. Molecular structure calculations

2.8.1. Molecular docking study

The molecular docking calculations were achieved by the AutoDock 4.2.6 program [28]. In the first step, the β- and γ-CyDs initial structures were prepared using the REDDB web server [22].

The RA structure was minimized by Gaussian 09 using the B3LYP/6-311++G(d,p) basis to achieve a stable geometry. The 40×40×40 Å and 46×46×46 Å dimensions (x, y, z) were set to for the β-CyD and γ-CyD grid boxes, respectively. The Lamarckian genetic algorithm (LGA) was used with energy evaluations, and the number of docking runs set to 25,000,000 and 250, in that order. The conformational cluster was performed according to the differences in the binding energy.

2.8.2. Molecular dynamics simulation

The molecular dynamics (MD) simulations were applied to the molecular docking poses of β- and γ-CyDs: RA ICs with minimal binding energy by using the AMBER (Assisted Model Building with Energy Refinement) software with the q4md-CD and GAFF force fields for CyDs and RA [29,30]. The partial charges to RA were assigned by the restrained electrostatic potential (RESP) method. The free (β- and γ-) CyDs and these ICs were solvated in a water box of a truncated octahedron with 10 Å dimensions, implementing the TIP3P model [31]. The energy minimization of the system was performed with the steepest descent algorithm for at least 10000 steps. The system was heated up to 300K as the equilibration step (NVT) to keep the pressure and the temperature constant, using the isotropic position scaling and the Berendsen thermostat method. The Particle-Mesh Ewald (PME) method was applied to preserve the long-range electrostatic interactions with 10 Å cutoff for van der Waals interactions and PME. Finally, the for 50 ns trajectory at constant temperature and pressure (NPT) was generated using the molecular mechanics generalized Born (MM-GBSA) or the Poisson-Boltzmann (MM-PBSA) surface area explicit solvation models to calculate binding affinity [32].

3. Results and discussions

3.1. The analysis of phase solubility

Due to RA with low solubility in aqueous media, the nutritional and therapeutic applications of this antioxidant are limited. Investigation of the effect of β- and γ-CyDs on the solubility of RA were performed and also calculated the apparent stability constant, K_C (eq. 1) [23,24]. As indicated in Fig. 1 and Fig. 2, with increasing concentrations of β-CyD and γ-CyD, the RA solubility increased linearly at the various temperatures (15, 18, 21, and 25 °C). Accordingly, solubility graphs represent the A_L group and the 1 to 1 stoichiometric ratio between guest (RA)

and host (CyDs) and. The values of K_C, $\Delta H^{o\prime}$, and $\Delta S^{o\prime}$ (Eqs. 1-3) for β-CyD: RA IC and γ-CyD: RA IC listed in Table 2. In keeping with the van't Hoff diagrams shown in Figs. 1-b and 2-b, the decrease in K_C with increasing temperature indicates that the process could be considered as an exothermic chemical reaction ($\Delta H^{o\prime} < 0$). This is as a result of the water molecules removal from the CyDs cavity. Furthermore, the negative entropy values ($\Delta S^{o\prime}$) indicate that the encapsulation of RA into the β- γ-CyD cavities ensued a decrease in the degrees of transitional and rotational freedom. As a result, the negative values of these two parameters and the driving forces of these IC formations represent the van der Waals interactions and hydrogen bonding as the dominant interactions. The stability order of the β- and γ-CyD: RA ICs with increasing K_C is as follows: β-CyD: RA IC > γ-CyD: RA IC. By comparing the stability of these complexes, it can be concluded that the β-CyD has a more suitable cavity size than that of γ-CyD. Therefore, it makes it a better candidate for its complexation with the RA molecule [22,33].

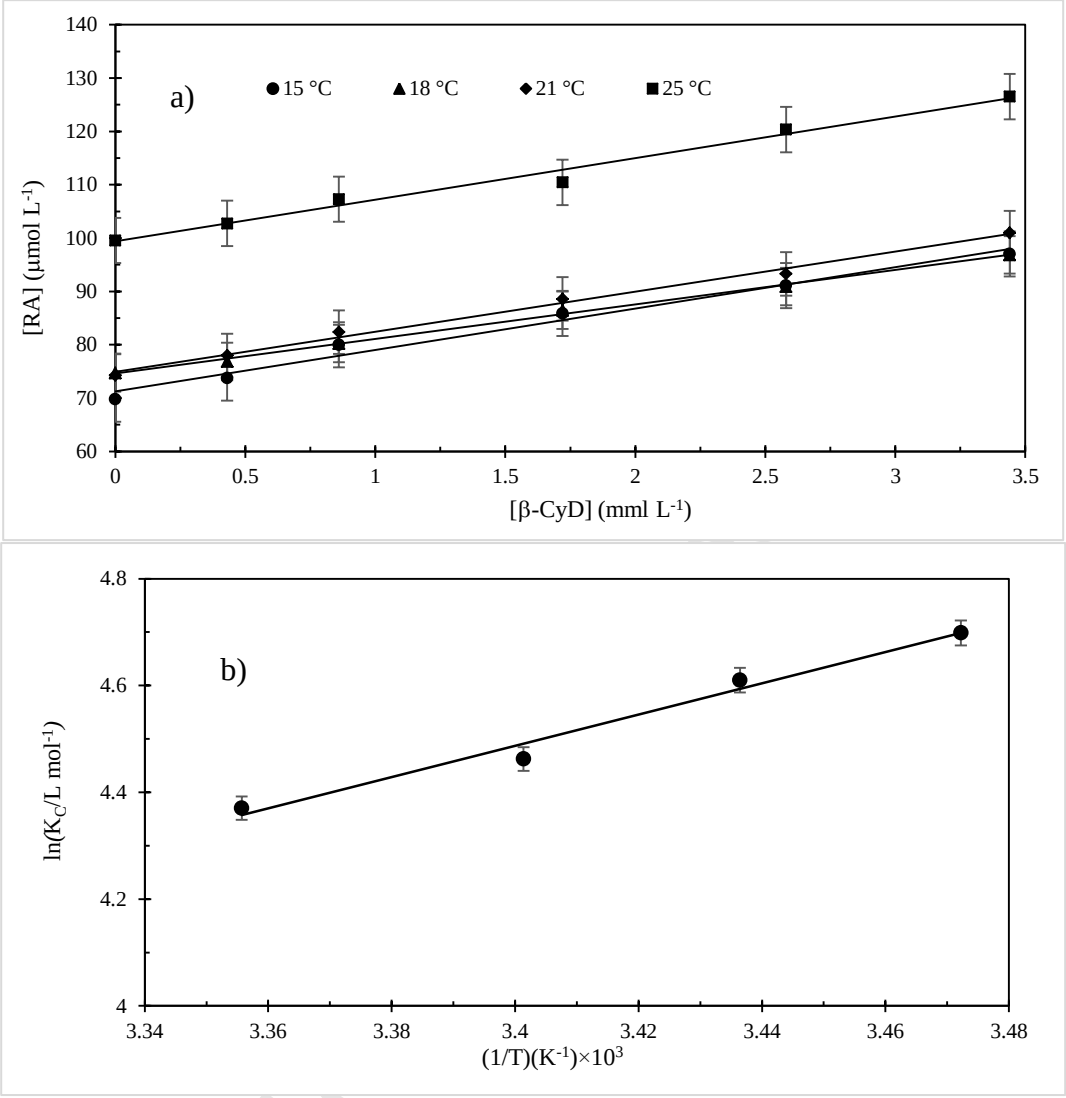

Fig. 1): a) The study of phase solubility in PBS (pH 7.4, 10 mmol L^{-1}) at several temperatures (15, 18, 21 and 25 °C; b) The van't Hoff plot, for the β-CyD: RA IC formation (R^2=0.982).

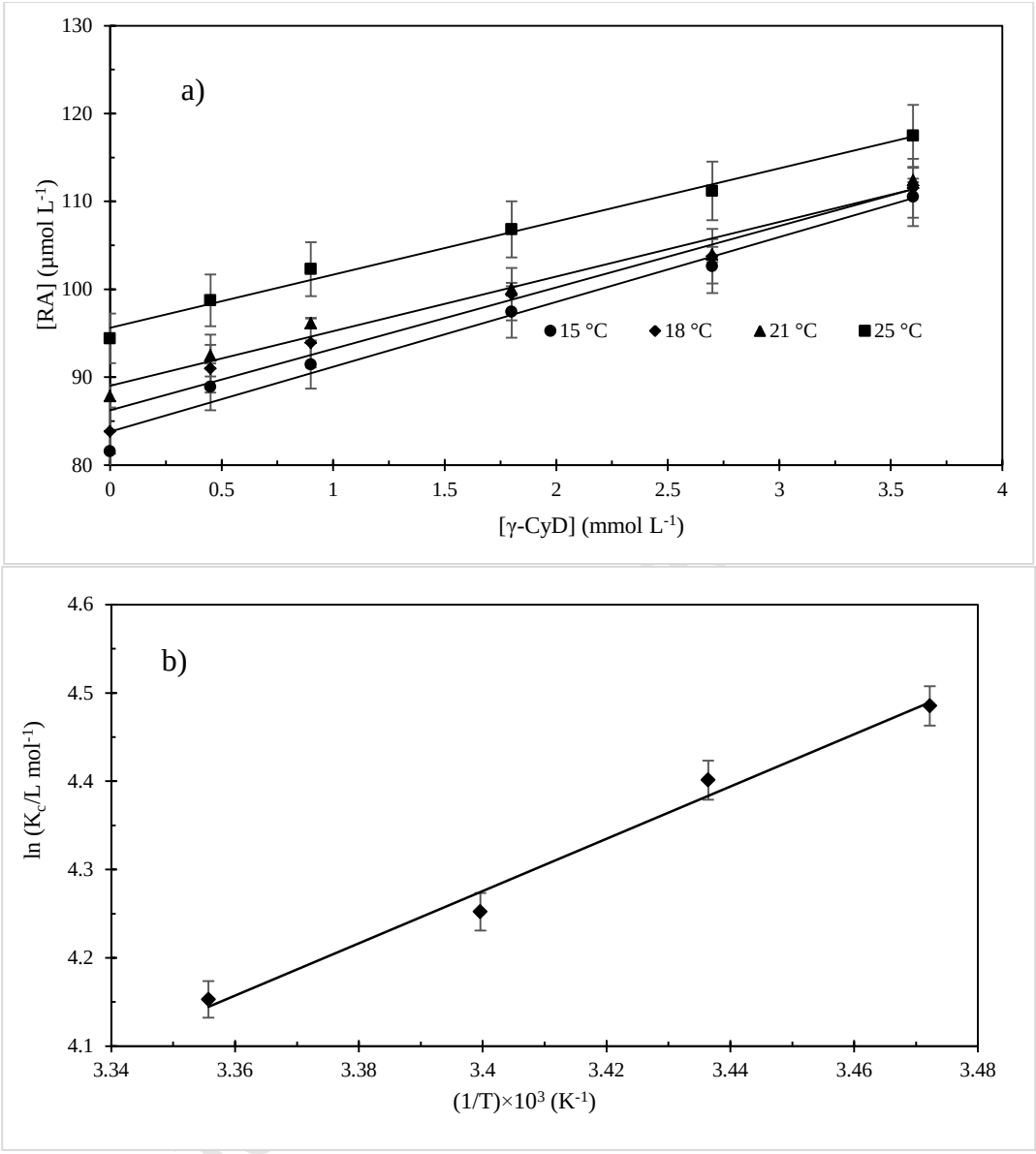

Fig. 2): a) The study of phase solubility in PBS (pH 7.4, 10 mmol L^{-1}) at several temperatures (15, 18, 21 and 25 °C; b) The van't Hoff plot for the γ-CyD: RA IC formation (R^2=0.983).

Table 2. a) The constants of phase solubility analysis (K_C) and the values of estimated thermodynamic for a) β-CyD: RA IC and b) γ-CyD: RA IC formation at several temperatures.

T (K)	S_o *(mol.L^{-1})*	slope	R^2	K_C (L mol^{-1})	$\Delta G^{0\prime}$/kJ mol^{-1}	$\Delta H^{0\prime}$/kJ mol^{-1}	$\Delta S^{0\prime}$/J K^{-1}mol^{-1}
288 ± 0.10	(7.11 ± 0.49) × 10^{-5}	(7.77 ± 1.02) × 10^{-3}	0.982	109.79 ± 7.10	-13.20 ± 0.08	-11.25 ± 0.31	-45.354± 1.49
291 ± 0.10	(7.49 ± 0.26) × 10^{-5}	(7.52 ± 0.86) × 10^{-3}	0.994	100.46 ± 4.48	-12.63 ± 0.72	-11.53 ± 0.17	-.45.22 ± 1.96
294 ± 0.10	(7.59 ± 0.17) × 10^{-5}	(6.41 ± 0.02) × 10^{-3}	0.997	86.70 ± 2.19	-12.00 ± 0.92	-10.91 ± 0.12	-45.59 ± 2.10
298 ± 0.10	(9.94 ± 0.10) × 10^{-5}	(7.80 ± 1.26) × 10^{-3}	0.986	79.07 ± 13.84	-11.42 ± 0.14	-10.83 ± 0.88	-45.25 ± 0.46

T (K)	S_o (mol L^{-1})	slope	R^2	K_C (L mol^{-1})	$\Delta G^{0\prime}$/kJ mol^{-1}	$\Delta H^{0\prime}$/kJ mol^{-1}	$\Delta S^{0\prime}$/J K^{-1} mol^{-1}
288 ± 0.10	(8.38 ± 0.10) × 10^{-5}	(7.38 ± 1.02) × 10^{-3}	0.980	88.70 ± 12.12	-10.74 ± 0.66	-24.60 ± 5.09	-48.13± 15.38
291 ± 0.10	(8.62 ± 0.46) × 10^{-5}	(6.98 ± 0.22) × 10^{-3}	0.974	81.55 ± 6.70	-10.65 ± 0.40	-24.60 ± 5.09	-.48.94 ± 16.13
294 ± 0.10	(8.90 ± 0.13) × 10^{-5}	(6.22 ± 0.37) × 10^{-3}	0.978	70.26 ± 5.31	-10.40 ± 0.37	-24.60 ± 5.09	-48.28 ± 16.04
298 ± 0.10	(9.56 ± 0.18) × 10^{-5}	(6.05 ± 4.15) × 10^{-3}	0.989	63.62 ± 9.31	-10.29 ± 0. 86	-24.60 ± 5.09	-48.02 ± 14.19

3.2. The β- and γ-CyD: RA inclusion complexes characterization

3.2.1. Spectroscopy of Fourier-transform infrared

The spectroscopy FT-IR is a valuable technique for characterizing CyD: Drug complexes. This method, in combination with other techniques, is used to entirely identify solid-state ICs and compare their structures with the separate host (CyDs) and guest (RA) components. As observed in Fig. 3, the FT-IR spectra for pure β-CyD, γ-CyD, RA, β- and γ-CyD: RA ICs were investigated as follows:

The spectra of FT-IR for Pure β-CyD and γ -CyD displayed in Fig. 3a-b, In these spectra, signified an outstanding absorption band at 3391 and 3396 cm^{-1} (the stretching vibrations of O-H, β- and γ-CyD, in that order), 1418 and 1439 cm^{-1} (the bending vibrations of O-H, β- and γ-CyD, respectively), the stretching and bending vibrations band for C-H (in CH_2 group) at 2927, 2931 and 1081, 935 cm^{-1} (β- and γ-CyD, respectively), the stretching vibration band for C-O and C-O-C in the ether linkage at 1157, 1155 and 1029, 1018 cm-1, (β- and γ-CyD), respectively [34].

The RA FT-IR spectrum (Fig. 3c) indicated an absorption band at 3458 and 1353 cm^{-1} (the stretching and bending vibrations carboxylic acid O-H), and 3309, 3174 and 3396 cm^{-1} (the stretching vibrations phenolic O-H), 1712 and 1678 cm^{-1} (acidic and esteric C=O stretching vibrations, respectively), 1610, 1520 and 1464 cm^{-1} (aromatic ring stretching vibrations) and also

the peak in 1259, 1074 and 1196 cm^{-1} was related to stretching vibrations for carboxylic acid, ester, and phenols, in turns.

The spectra of β-CyD: RA IC (Fig. 3d) demonstrated absorption bands in 3375 cm^{-1} (for O-H stretching vibrations) with redshift, and the reduced intensity compared to the spectrum showed for β-CyD. It is important to note that the –OH spectra of phenolic and carboxylic acid are covered by –OH spectra of β-CyD. The –CH groups stretching vibrations in 2929 cm^{-1} were accompanied by blue shift and increased intensity, indicating the presence of the –CH group in β-CyD and RA. Also, the characteristic bands of RA in IC included 1709 cm^{-1} (for C=O carbonyl groups stretching vibrations) with redshifts and the reduced intensity pure RA and the ether linkage of O-C-O in complexed β-CyD with 1030 cm^{-1} along with reduced intensity and C-O esteric, carboxylic acid and phenolic groups stretching vibrations in 1610, 1592 and 1480 cm^{-1}, respectively, with reduced intensity. This spectral changes such as intensity and blue or redshift might be because of the incorporation of RA into β-CyD hydrophobic cavity.

The γ-CyD: RA IC spectra (Fig. 3e) revealed absorption bands in 3381 and 1633 cm^{-1} (for O-H stretching and bending vibrations) with redshift and the reduced intensity compared to the spectrum observed for pure γ-CyD. It is important to note that the –OH spectra of phenolic and carboxylic acid are covered by –OH spectra of γ-CyD. The –CH groups stretching vibrations in 2927 cm^{-1} were accompanied by blue shift and increased intensity, indicating the presence of the –CH group in γ -CyD and RA. Also, the characteristic bands of RA in IC included 1707 cm^{-1} (for C=O carbonyl groups stretching vibrations) with redshifts and the reduced intensity pure RA and the ether linkage of O-C-O in complexed γ-CyD with 1028 cm^{-1} along with reduced intensity and C-O esteric, carboxylic acid and phenolic groups stretching vibrations in 1604, 1520 and 1448 cm^{-1}, respectively, with reduced intensity. This spectral changes such as intensity and blue or redshift might be because of the incorporation of RA into γ-CyD hydrophobic cavity. In general, the spectral changes (red or blue shift in wavenumber, sharpening, decreasing, or flattening spectra intensities) can approve the β- and γ-CyD: RA ICs. This data designates changes in the drug environment due to the van der Waals interactions and hydrogen bonding formation between -OH phenolic groups of RA and the -OH groups of CyDs.

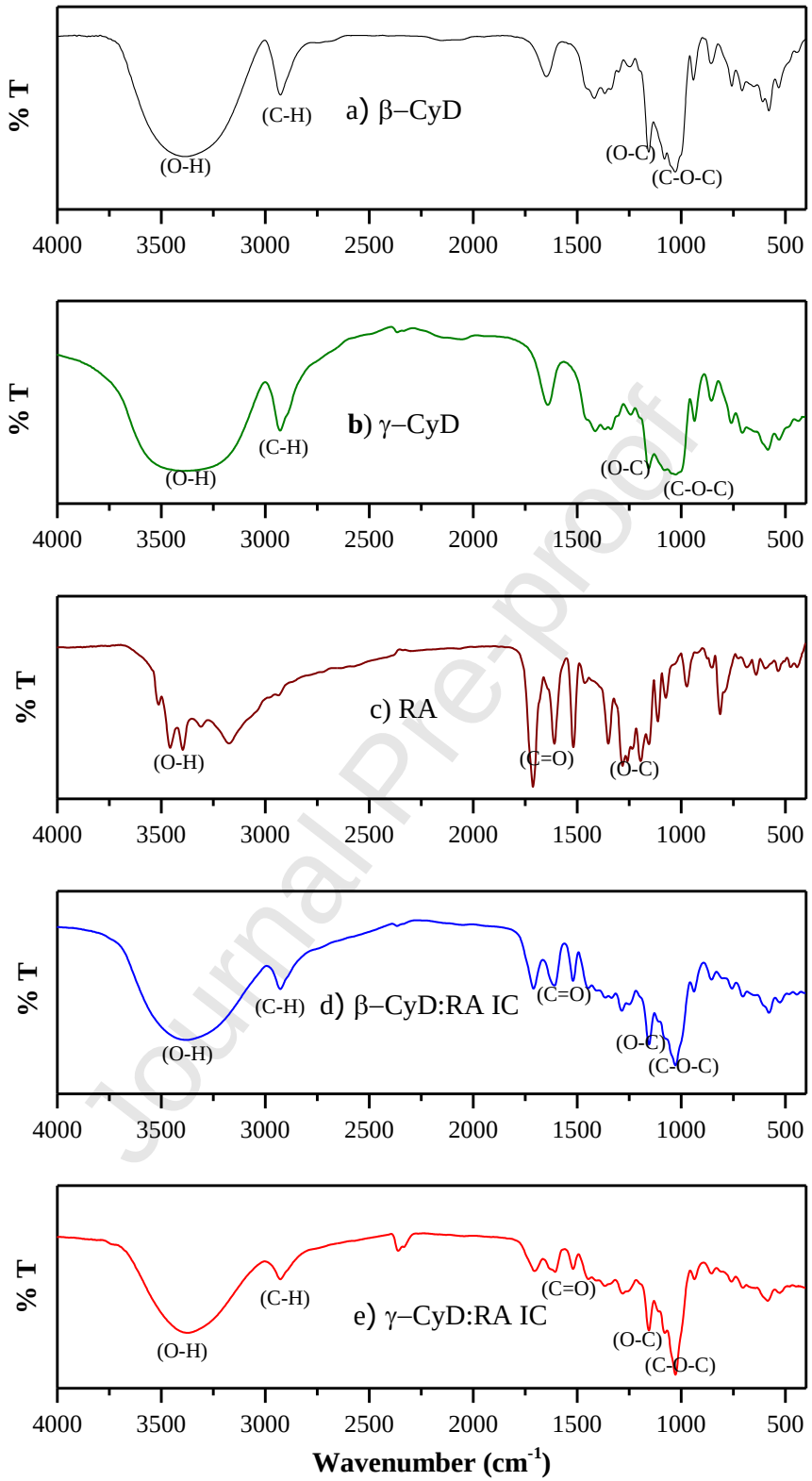

Fig. 3): The spectra of FT-IR of a) β-CyD, b) γ-CyD, c) RA, d) β-CyD: RA IC, b), e) γ-CyD: RA IC.

3.2.2. The spectroscopy of ^{1}H-Nuclear magnetic resonance

The spectroscopy of ^{1}H-NMR is a valuable technique for the analysis of chemical shift changes in the complexation, and the main difference pure guest and host and IC formed between those [35]. The H-5 and H-3 located into the narrower part and broader part of the cavity of β- and γ-CyD, respectively. So, these two protons display chemical shifts by the insertion of the guest into the cavities of CyD. As shown in Fig. ESI 1, the ^{1}H-NMR spectra of the free β-CyD, γ-CyD, and RA with the insertion of RA into the cavity of β- and γ-CyD were compared and assessed changes of chemical shift between those. Fig. ESI 1a demonstrates the value of 3.93 and 3.83 for H-3 and 5 in pure β-CyD. While the ^{1}H-NMR spectrum for the β-CyD: RA IC (Fig. ESI 1-d) displays 3.82 ppm for H-3 (Δδ= -0.09 ppm), 3.66 ppm for H-5 (Δδ= -0.17 ppm) and the most change of chemical shift for H-8' in RA is Δδ= -0.05 ppm (5.23 ppm in free RA and 5.18 ppm in complexed RA). The results of chemical shift changes are observed in Table 3a. The most observable change of chemical shift is indicated for H-5 and H-8' (carboxylic acid). As a result, it could be concluded that the acidic group inserted into the cavity of β-CyD. Therefore, the ^{1}H-NMR study approves IC is formed and inserted RA into the β-CyD cavity. In the case of γ-CyD: RA IC, Fig. ESI 1-b and e indicate the values of 3.84 and 3.73 ppm (Δδ= -0.11 ppm) and these values for H-5 in pure and complexed γ-CyD are 3.58 and 3.64 ppm (Δδ= 0.06 ppm), respectively. Furthermore, the most chemical shift change for H-7 in RA in free RA and 5.18 ppm in complexed RA are Δδ= -0.30 ppm. According to the data mentioned above, H-3 and H-7 in γ-CyD and RA display the maximum values for Δδ representing the insertion of RA into the γ-CyD cavity and formation of the γ -CyD: RA.

Table 3. ^{1}H-chemical shift (δ [ppm]) for a) free β-CyD, RA and β-CyD: RA IC and b) γ-CyD, RA and γ-CyD: RA IC in D_2O at 25 °C

a) β-CyD	**$\delta_{\beta\text{-CyD}}$ /ppm**	**$\delta_{complex}$ /ppm**	**Δδ /ppm**
H-1	5.02	4.96	-0.06
H-2	3.60	3.55	-0.05
H-3	3.93	3.82	-0.11
H-4	3.55	3.50	-0.05
H-5	3.83	3.66	-0.17

H-6	3.84	3.73	-0.11
RA	**δ_{RA} /ppm**	**$\delta_{complex}$ /ppm**	**Δδ /ppm**
H-2	7.05	7.04	-0.01
H-2'	6.77	6.76	-0.01
H-5	6.87	6.84	-0.03
H-6	6.94	6.97	+0.03
H-6'	6.74	6.70	-0.04
H-7	7.46	7.49	0.03
H-8	6.22	6.23	0.01
H-8'	5.23	5.18	-0.05
b) γ-CyD	**$\delta_{\gamma\text{-CyD}}$ /ppm**	**$\delta_{complex}$ /ppm**	**Δδ /ppm**
H-1	5.03	4.98	-0.05
H-2	3.56	3.61	0.05
H-3	3.84	3.73	-0.11
H-4	3.51	3.48	-0.03
H-5	3.58	3.64	0.06
H-6	3.77	3.72	0.05
RA	**δ_{RA} /ppm**	**$\delta_{complex}$ /ppm**	**Δδ /ppm**
H-2	7.05	6.78	-0.27
H-2'	6.77	6.67	-0.01
H-5	6.87	6.69	-0.18
H-6	6.94	6.71	-0.23
H-6'	6.74	6.58	-0.16
H-7	7.46	7.16	-0.30
H-8	6.22	6.24	0.02
H-8'	5.23	5.49	0.26

3.2.3. Scanning electron microscope

One of the essential techniques of investigation of ligands, CyD, and their ICs is the SEM method. The micrographs of pure RA, β- and γ-CyD, and ICs of β- and γ -CyDs: RA are showed in Fig. 4. As observed in Fig. 5 a and b, β- and γ -CyD indicated the quadrilateral form, and RA

has a rod-shaped crystal. The β- and γ-) CyDs: RA ICs appeared as irregularly amorphous fragments and various dimensions that seem to be due to the relative difference in size and shape of RA, β-CyD, and γ -CyD. For that reason, these analyses could be proved the existence of a new solid phase, indicative of the ICs of β-CyD: RA and γ -CyD: RA formation [36,37].

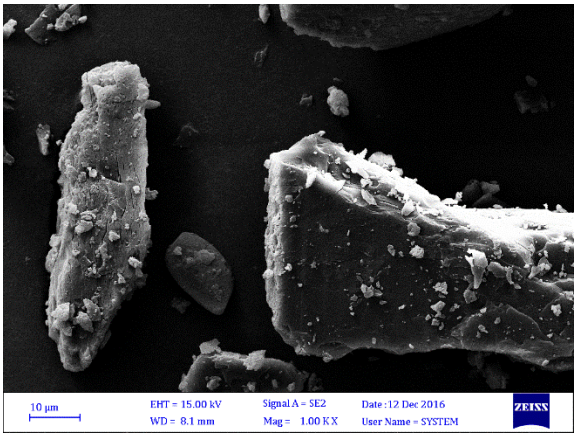

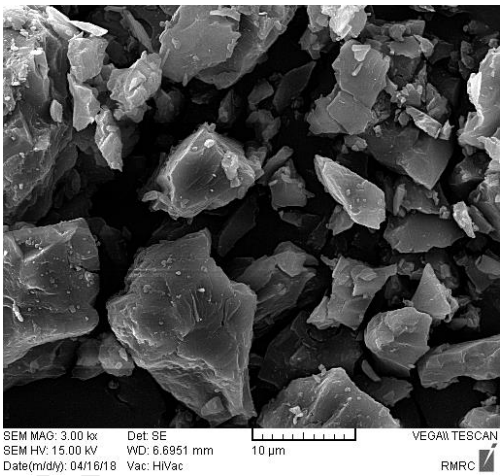

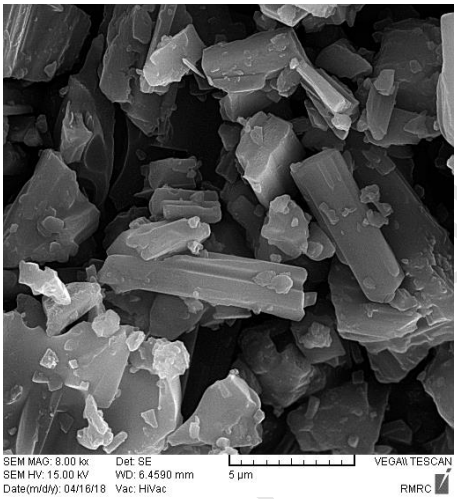

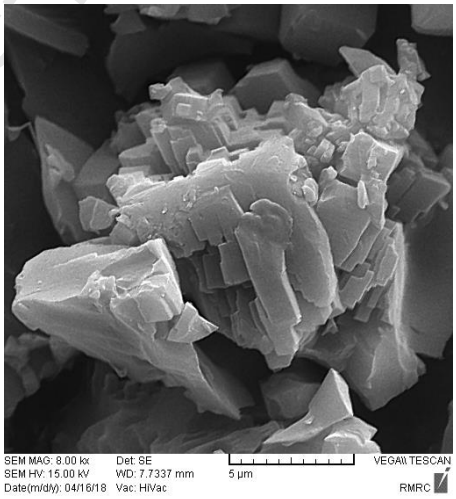

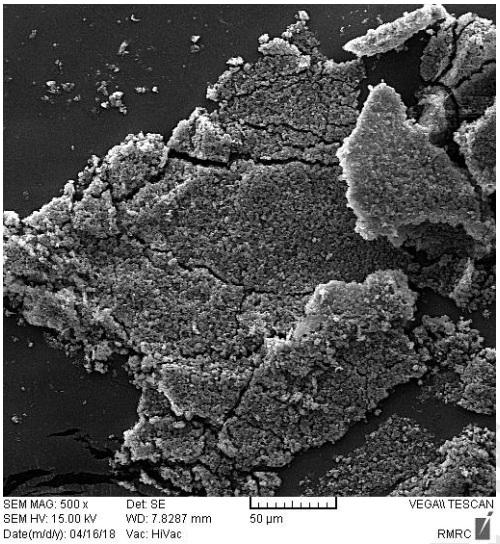

Fig. 4): The SEM micrographs for a) β-CyD, b) γ-CyD, c) RA, d) β-CyD: RA IC and e) γ-CyD: RA IC.

3.2.4. X-ray diffraction

The XRD technique was applied to confirm the formation of ICs between CyDs and RA. The XRD diffractograms for β-CyD, γ-CyD, RA, β-CyD: RA IC, and γ-CyD: RA have been observed in Fig. 5. Fig. 5-a and b describe the intensity peaks at different diffraction angles (2q) of 10.35, 14.65, 14.70, 14.75, 22.75, and 40.65° for β -CyD and 12.10, 12.20, 16.24, 16.35, 18.75 and 21.88° for γ-CyD. Also, the RA diffractogram (Fig. 5-c) shows several peaks with various angles and intensities in 13.48, 14.94, 14.98, 19.46, 19.48, 23.98, 26.36 and 28.72° that these high-intensity peaks at different diffraction angles indicate the crystalline nature of this drug compound. The XRD peak of β-CyD: RA IC and γ-CyD: RA IC have been observed in Fig. 5-d, and e. Two diffractograms for these ICs showed the pattern associated with the amorphous structure after the freeze-drying procedure.

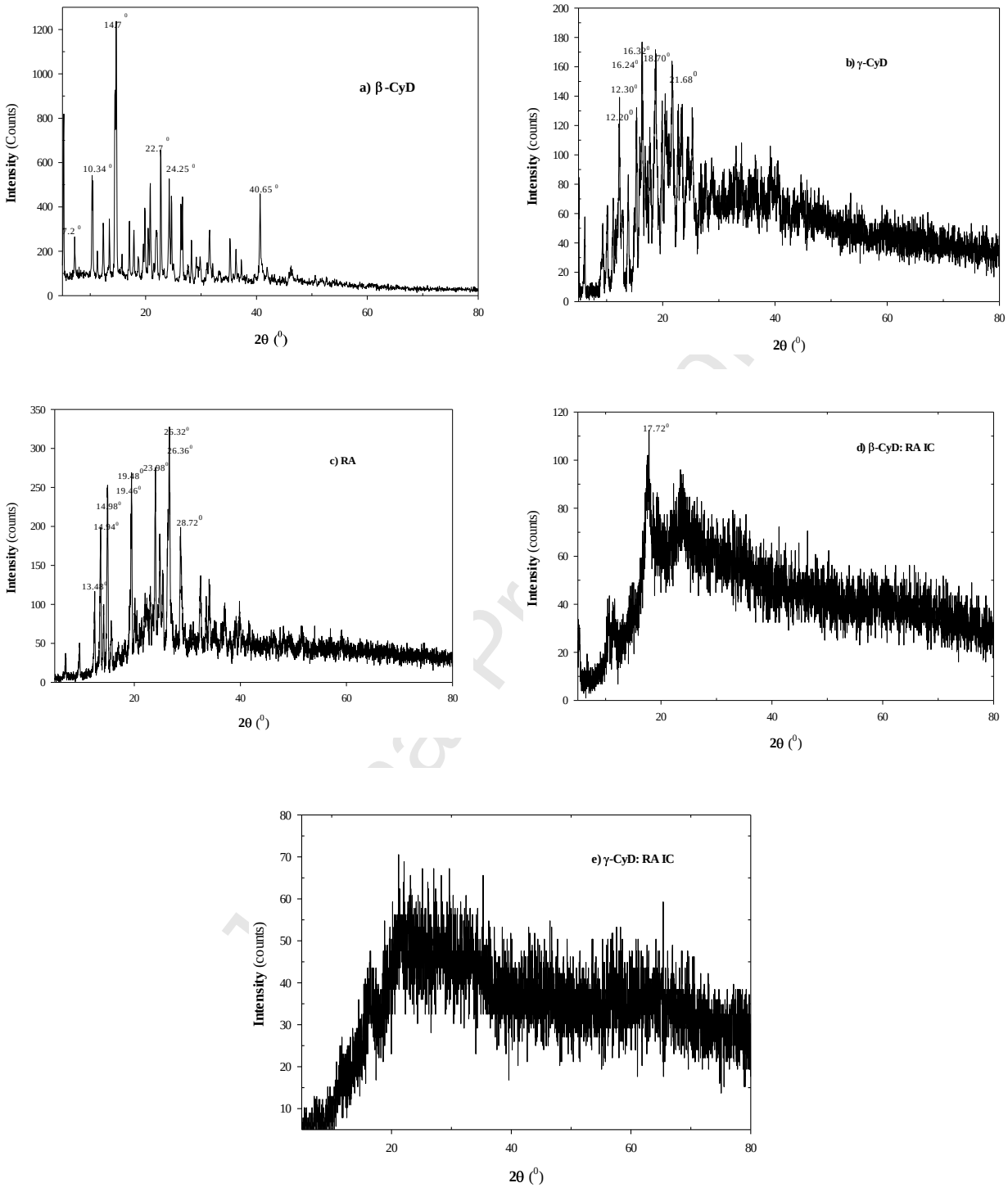

Fig. 5): X-ray diffractograms for a) β-CyD, b) γ-CyD, c) RA, d) β-CyD: RA IC and e) γ-CyD: RA IC

3.2.5. The spectroscopy of induced circular dichroism (ICD)

The ICD spectroscopy is one of the techniques to evaluate the molecular recognition in the formation of IC between CyDs and optically active molecules of a guest. As a result, this technique could point to the ICD peak presence for the insertion of optically active guest molecules into the CyDs cavity [38]. The spectra for β-CyD, γ-CyD, RA, β-CyD: RA IC, and γ-CyD: RA have been indicated in Fig. 6. The ICD spectrum for RA displays a positive peak in 294 nm with $\Delta\varepsilon$= 44.04 L mol^{-1} cm^{-1}. As is evident in this Fig. 6, the ICD spectra for β-CyD: RA IC and γ-CyD: RA IC seems to be positive ICD at 298 and 304 nm with $\Delta\varepsilon$= 22.01 and 17.10 L mol^{-1} cm^{-1} indicative of the insertion of RA into the cavities of these two CyDs. These positive peaks indicate the parallel or diagonal insertion of RA into the cavity of these CyDs.

3.3. Encapsulation efficiency and loading capacity

The EE% and LC% values for ICs of β-CyD: RA and γ-CyD: RA obtained using the freeze-drying process was evaluated by UV-vis spectroscopic measurements at 324 nm. Concerning Eqs. 5 and 6, the values of (24.014 ± 4.030) % and (23.505 ± 1.730) % were obtained for LC% (mg of encapsulated RA/mg of complex powder) ×100) for β-CyD: RA IC and γ-CyD: RA IC, respectively and also the amounts of (83.220 ± 13.970) % and (76.340 ± 5.620) % were calculated EE% for (β- and γ-CyD): RA ICs, respectively.

LC % and EE % values for locating of RA into the β-CyD cavity are higher than that for γ-CyD, which may be because of the size of the cavity in β-CyD better than γ-CyD.

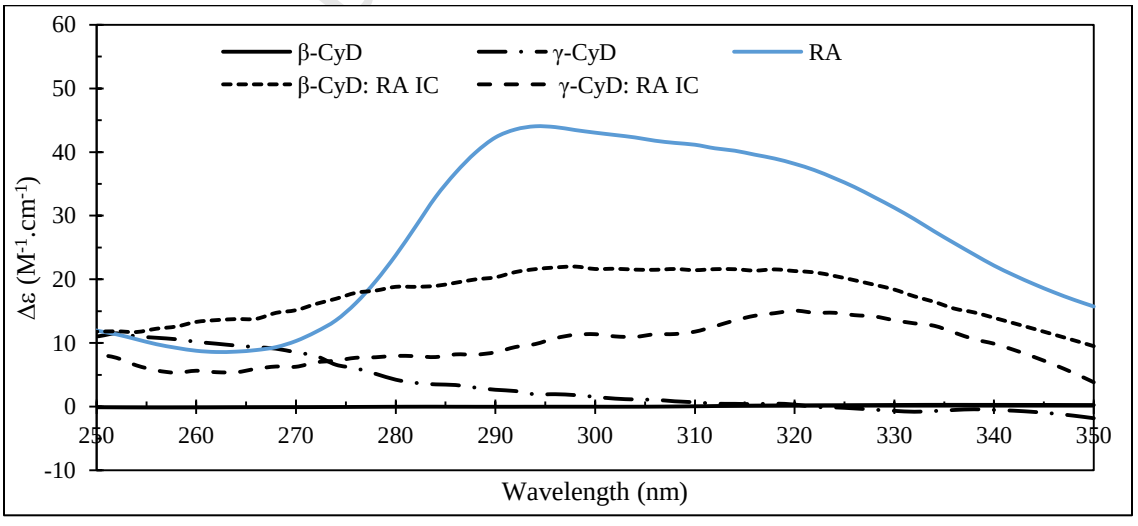

Fig. 6: The ICD spectra for a) β-CyD, b) γ-CyD, c) RA, d) β-CyD: RA IC, and e) γ-CyD: RA IC.

3.4. Photo-stability analysis

The photo-stabile investigations of polyphenol compounds are essential in various fields of science and technology, such as pharmaceutical industries. The hydrogen atoms in photosensitive phenolic groups in polyphenol compounds such as RA can be radicalized, and therefore this antioxidant has low stability in several environmental conditions e.g., light, oxygen, and moisture. As a result, the protection and improvement of this photosensitive compound versus physical agents are necessary and recommended. [39]. The insertion of RA could improve the photo-stability of RA into the β- and γ-CyD cavities. So, the photo-degradation reaction was monitored spectrophotometrically for pure and complexed states of RA in aqueous media with exposure to UVC lamp.

The apparent rate constant (*k*) for the RA photo-degradation as a pseudo first-order reaction has been valued along with the following equation:

$$\ln\left(\frac{A_t}{A_0}\right) = -kt \qquad (8)$$

Where A_t and A_0 and are the UV-vis spectroscopy absorption at initial and after exposure to UVC lamp in aqueous media at 324 nm, and t is time, respectively. Fig. 7 shows the variation of ln (A_t/A_0) *vs.* time for pure RA and β- and γ-CyDs: RA ICs. The values of *k* and $t_{0.5}$ (half-life time) were listed in Table 4.

Based on the results presented in Table 4, the photo-stability of pure RA and its ICs is as follows:

RA < γ-CyD: RA < β-CyD: RA

These results show that the insertion of RA into the β-CyD and γ-CyD cavities have mostly protected this compound against UV light and improved photostability and reduced the photo-degradation of RA. According to these results, the γ-CyD: RA IC showed less photo-stability than the β-CyD: RA IC. The reason is that the cavity of γ-CyD is larger than β-CyD cavity and the rotation of the RA into the γ-CyD cavity.

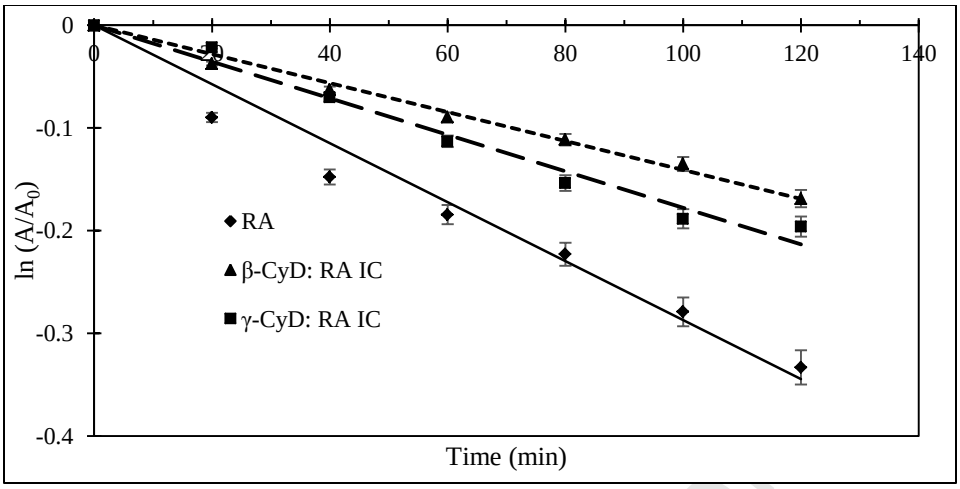

Fig. 7): The photo-degradation plots for free RA (♦), β-CyD: RA IC (▲) and γ-CyD: RA IC in the variation of ln (A_t/A_0) *vs.* time (min) in aqueous media after the exposure to UVC lamp, where A_0 and A_t are the UV–vis absorption spectroscopy at 324 nm at initial and after exposing to UVC lamp in aqueous media, respectively.

Table 4: The apparent pseudo first-order rate constant (*k*) and the half-life time ($t_{0.5}$) for photo-degradation reaction of RA, (β- and γ-) CyDs: RA ICs in aqueous media after the exposure to UVC lamp.

Aqueous media (UVC lamp)	***k* (×10^3) (min^{-1})**	**$t_{0.5}$ (min)**
RA	2.87 ± 0.1	24146 ± 16.87
β-CyD: RA IC	1.41 ± 0.24	491.84 ± 17.39
γ-CyD: RA IC	1.78 ± 0.03	389.76 ± 6.93

3.5. Antioxidant activity

The presence of phenolic hydroxyl groups causes antioxidant activity (AC) in RA. Because of the electron-donating hydrogen atoms, these groups act as free radical stabilizers. As shown in Fig. 8, the results of AC for pure β-CyD, γ-CyD, RA, Trolox, and the β-CyD: RA and γ-CyD: RA complexes are shown in Fig. 8. $ABTS^{\bullet+}$ radical scavenging % was measured using Equation

7. As a reducing sugar, it would be expected that free β- and γ-CyDs did not display any AC, and their $ABTS^{\bullet+}$ radical scavenging % was in the variety of 9.66 to 16.63 and 15.58 to 24.81 % for β-CyD and γ-CyD, respectively. Therefore, the AC observed for these compounds can be due to interference with other components in the solution, and the interpretations should not be regarded as an absolute value for them. Also, due to the small changes seen in CyDs, the higher concentrations of these compounds are not recommended in the industry. The antioxidant activity of RA increases significantly from ~45.45 to 95.51% (~ 50%) by increasing its concentration from 30 to 90 μmol L^{-1}.

The masking effect on the AC was calculated for the encapsulated RA into the CyDs cavity. The masking effect for the β- and γ-CyD: RA ICs was 12.17 to 20.04%, and 22.74 to 23.82%, respectively. The AC masking values are dependently on the binding affinity of RA to β-and γ-CyD [35,36]. By incorporation of RA into the CyD cavities, the AC of pure RA has a slight decrease at all studied concentrations of RA. The AC changes of RA may be due to the formation of intermolecular H-bonding of the RA with the -OH groups in CyDs in the β- and γ-CyD: RA ICs. Therefore, it can be deduced that the formation of β- and γ-CyD:RA ICs can cause masking of some hydroxyl groups of RA. When RA is encapsulated with CyDs, ortho-phenolic groups in this antioxidant are incorporated into the non-polar cavity and thus result in the oxidation-reduction behavior of the RA compound [40–42]. Also, the insertion of RA into the hydrophobic and less-polar of CyD cavities not only protects this compound from environmental damage such as light, oxygen, moisture, and rapid oxidation but also significantly enhances its solubility in its free state. As a result, the increase in aqueous solubility and protection of this compound may justify the profound difference in AC of RA compared to the β- and γ-CyD: RA ICs.

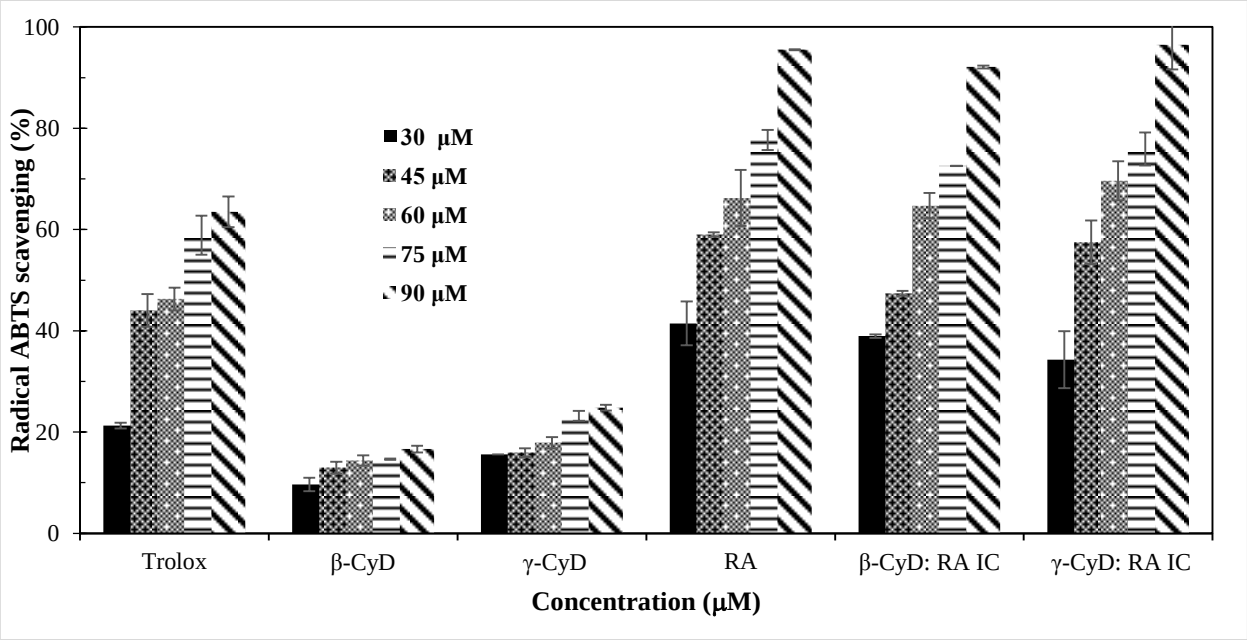

Fig. 8): The antioxidant concentration effects on the $ABTS^{\bullet+}$ inhibition

3.6. Computational methods

3.6.1. Molecular docking analysis

In this study, the interaction of RA into the β- and γ-CyD cavity have been evaluated by molecular docking. The incorporation of drugs into these CyD cavities, the free binding energies, and the number of hydrogen bonds in these interactions are also reported. Finally, the molecular docking results of two CyD types were compared. At the end of each molecular docking calculation, 250 different configurations of RA are generated. Then, these RA configurations based on the RMSD of the corresponding atoms are clustered and arranged in energy order. In the case of RA, the configuration with the lowest energy and the largest population is selected as the main configuration [43].

In the β–CyD: RA IC formation, four hydrogen bonds are observed for the RA and β-CyD interaction. These hydrogen bonds include a) The phenolic H (C4) of RA molecule with the O of -OH (C-6) glycopyranoside unit (No. 1); b) The phenolic H (C3') of RA with O4 glycopyranoside unit (No. 2), c) The H of –OH in phenyl ring (C4') with O of -OH (C-2) glycopyranoside unit (No. 1) and d) The O of phenolic -OH (C4') with O of -OH (C-3) glycopyranoside unit (No. 1). In this molecular docking job, 37 clusters were observed for the orientation of RA into the β-CyD cavity and the RA configuration with the largest population

and lowest energy of -5.97 kcal mol^{-1} selected as the main orientation of RA into the β-CyD cavity. These results of molecular docking for the orientation of RA into the β–CyD cavity are in agreement with spectroscopies of ^{1}H-NMR and ICD. (See in Fig. 9-a).

As observed in Fig. 9-b, the results of molecular docking calculations in the γ–CyD: RA IC formation indicated three hydrogen bonds for the encapsulation of RA into γ-CyD cavity. These hydrogen bonds are formed between the two H-phenolics (C3' and C4') of RA antioxidant with the O4 glycopyranoside unit (No. 5) and the H-phenolic (C3) with O of –OH (C6) glycopyranoside unit (No. 8). In this molecular docking analysis, 45 clusters were indicated for the orientation of RA into the γ-CyD cavity and the RA configuration with the largest population and lowest energy of -6.06 kcal mol^{-1} selected as the primary orientation of RA into the γ-CyD cavity. These results of molecular docking for the orientation and encapsulation of RA into the γ-CyD cavity align with the results of two spectroscopies ^{1}H-NMR and ICD.

Concerning the results of molecular docking for the interactions of β- and γ-CyDs with RA, it can be concluded due to the large size of the RA compound, the free binding energy of interaction of RA with γ-CyD is higher than that of β-CyD. It should be noted, however, that in the interaction of β-CyD with RA, the number of hydrogen bonds is more than these of γ-CyD: RA IC, so this interaction is more stable.

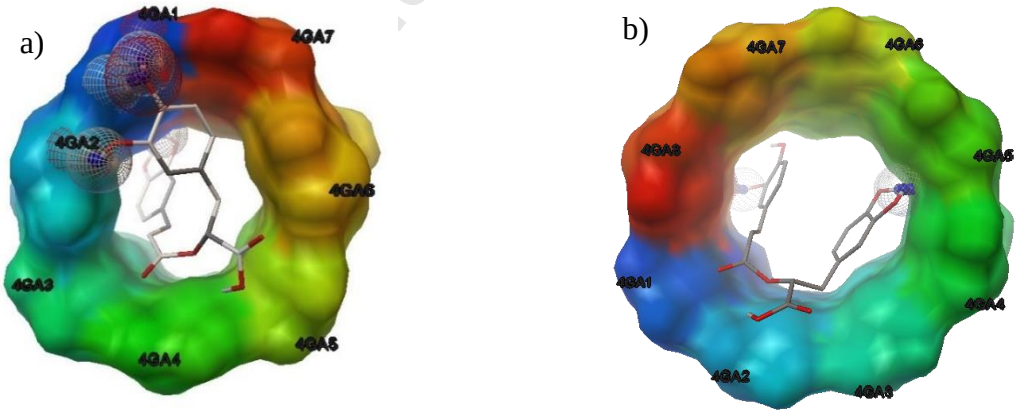

Fig. 9): The molecular docking structures for a) β-CyD: RA IC and b) γ-CyD: RA IC.

3.6.2. Molecular dynamics simulation

The computational results of MD simulations provided evidence that CyDs can form stable ICs with RA in aqueous media. The MD simulations in water box were accomplished to explore the conformational change of RA molecule within the of β- and γ-CyD cavities for 50 ns at room

temperature. For that, we used the root mean square displacement (RMSD), root mean square fluctuation (RMSF), radial distribution function (RDF), solvent accessible surface area (SASA), and the distance between the RA center of gravity and β- and γ-CyDs. Additionally, the MM-PBSA and MM-GBSA scripts were executed to evaluate the binding affinity together with the enthalpy-entropy compensation [44]. As shown in Fig. 10, the conformational changes were observed for β- and γ-CyDs in a free and bound state during the 50 ns trajectory. The RA molecule was imbedded into the binding cavities of both CyDs supporting the data from the ^{1}H-NMR and molecular docking experiments [45].

To compare the stability of β- and γ-CyDs: RA IC after the encapsulation, we have computed RMSD of the β- and γ-CyDs corresponding to those of the initial structure from docking, in free and complex state and then the stabilities of all structures during 50 ns were studied [46]. The RMSD for β- and γ-CyDs in free and IC states have been observed in Fig. 11. In these Figs., the RMSD values of β- and γ-CyD in the free state (blue) and complexed state (red) have been presented during the simulation time. The mean values of RMSD for β-CyD in the pure and complexed states were 0.848 ± 0.224 Å and 2.157 ± 0.496 Å and for the free and IC states in γ-CyD were 1.043 ± 0.336 Å and 1.997 ± 0.314 Å, respectively. The RMSD values for β- and γ-CyDs and β- and γ-CyDs: RA IC agreed with the results of snapshots of configuration changes in Fig. 10. From Fig. 11-c, the RMSD values for RA in the first IC (β-CyD: RA IC) are lower (RMSD = 1.392 ± 0.421 Å) than for RA (RMSD = 1.493 ± 0.659 Å) in the second one (γ-CyD: RA IC), indicating the restrictive effect of the β-CyD binding cavity. In other words, the more extended γ-CyD binding site permits more flexibility for RA than β-CyD. The comparison of the structural changes (Fig. 10) and RMSD behavior (Fig. 11) lead us to conclude that RA forms a more stable IC with β-CyD than γ-CyD.

0 ns	10 ns	25 ns	40 ns	50 ns
a) β-CyD (Free)				
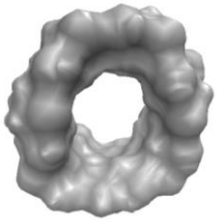	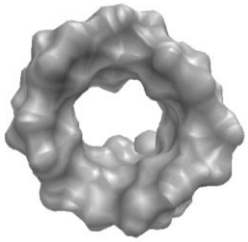	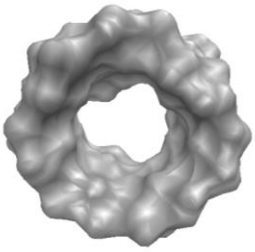	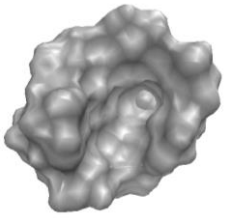	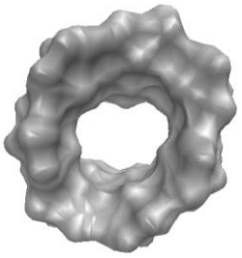
β-CyD: RA IC				
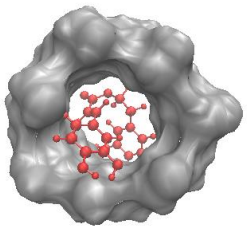	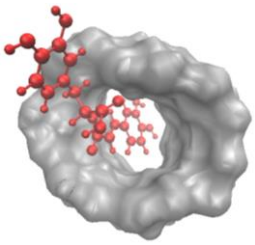	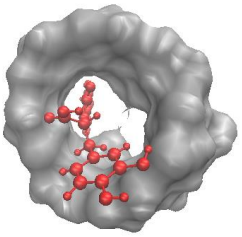	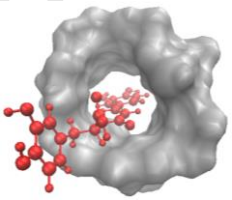	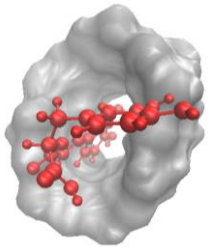
b) γ-CyD (Free)				
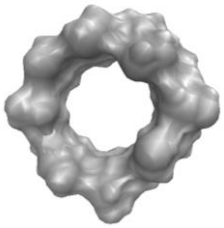	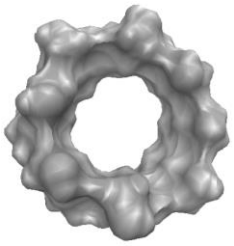	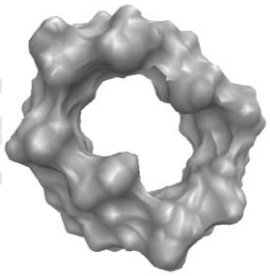	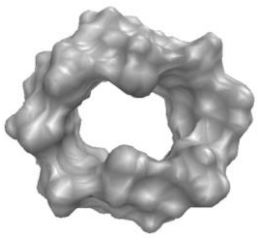	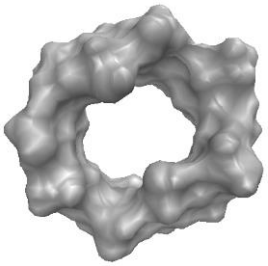
γ-CyD: RA IC				
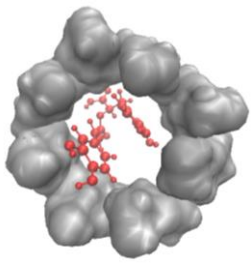	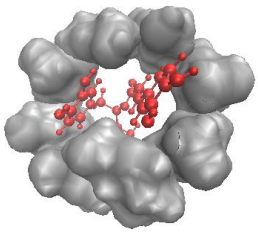	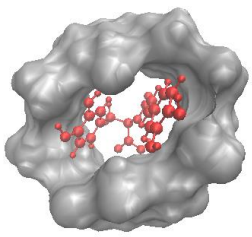	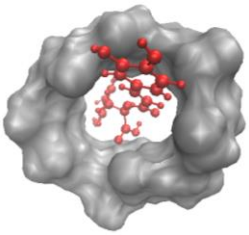	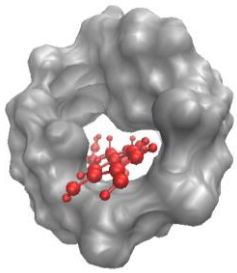

Fig. 10): Snapshots of in the pure and complexed states of a) β-CyD and b) γ-CyD with RA at the several times 0, 10, 25, 40, and 50 ns.

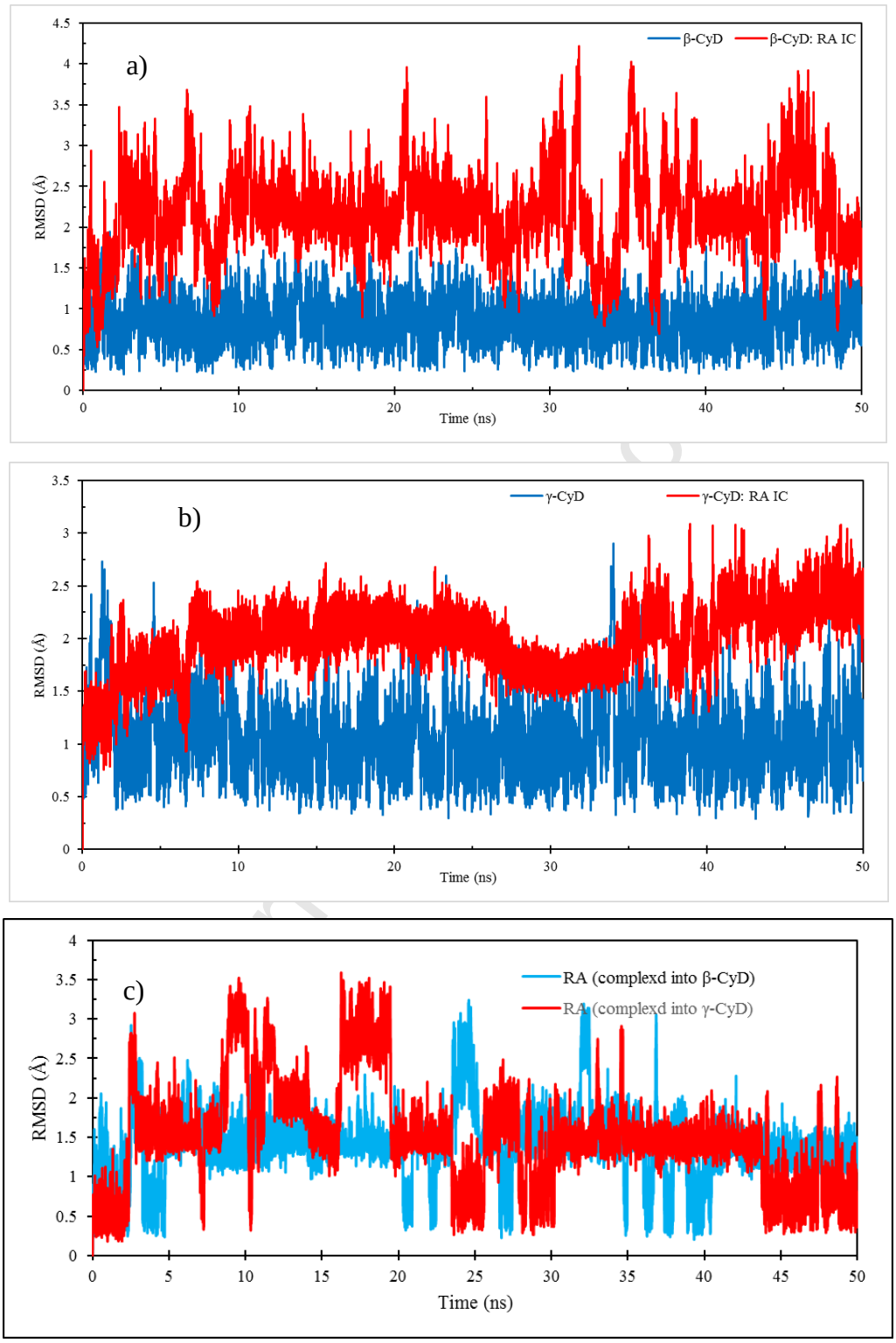

Fig. 11): RMSD of free and IC states for a) β-CyD, b) γ-CyD with RA, and c) RA in IC states for 50 ns simulation time.

RMSF analysis for β- and γ-CyD to evaluate the atoms in a glycopyranoside unit in the presence and absence of RA and the water solution in Fig. ESI 2 was investigated. In these CyDs, the highest fluctuations are observed for the H6O, O6 (H and O in –OH of C6), H61 and H62 atoms (see scheme 1a), which may be due to flexibility of primary hydroxyl group (-OH6). In both CyDs, the fluctuations of all atoms in the studied glucose unit in the complexed state were more significant than in the free state β- and γ-CyD. Also, the fluctuations in the RMSF complex β-CyD: RA IC were more significant than the γ-CyD: RA. These results were in agreement with the RMSD and snapshots.

The binding and Dynamic Behavior of β- and γ-CyDs complexation with RA, the O4-O5 distance in glycopyranoside unit of β- and γ-CyDs and also the center of mass (CoM) of RA to O4-(β- and γ-) CyDs for the duration of 50 ns simulation time in Table 5-a were investigated. As can be indicated in Fig. ESI 3, the fluctuation of O4-O5 distance for β- and γ-CyDs in the absence and presence of RA were not noticeable during the 50 ns simulation time. So it can be concluded that in these CyDs, with complexation, no significant configuration change was observed. This claim is confirmed in Fig. 10. Furthermore, the initial, final, and mean of O4-CyDs:RA IC values were shown in Table 5-b. In β- and γ-CyD: RA IC, the average distance is not significantly different from the initial values, and indicating a stable IC formation between these CyDs and RA. (See Fig. ESI 4).

Table 5: a) The distance of O4-O5 in CyDs in the free and complexed states with RA, and b) the O4-CyDs values of initial, average and final in (β- and γ-CyD): RA during the simulation time

a) The distance (Å) of (O4-O5) in CyD free and complex forms with RA			
β-CyD: RA	1.261 ± 0.110	β-CyD (free)	1.247 ± 0.112
γ-CyD: RA	1.114 ± 0.096	γ-CyD (free)	1.618 ± 0.112

b) O4-CyDs (β- and γ-CyD): RA			
Inclusion complex	Average Distance (Å)	Initial value (Å)	Final value (Å)
β-CyD: RA	1.436 ± 0.767	1.852	0.570
γ-CyD: RA	5.314 ± 0.557	5.557	5.219

RDF plots to investigate the pairwise correlation functions (g(r)) between the oxygen atoms of the water molecules, with the oxygen atoms of the β-CyD, γ-CyD, and RA molecules in pure and complexed states are illustrated in Fig. 12, and Fig. ESI 5. As observed in Fig. 12-a, b, and Fig. ESI 5-a, b, the RDF diagram of the oxygen atoms O2, O3, O4, O5, and O6 of the β- and γ-CyD compound in the free state and complexed with RA, show a very similar structure. However, the intensity of the peaks in the complexed state was lower than that of the CyDs in the free state. This relatively small decline in peak intensity maybe since the molecules of water are released from the CyDs cavity and the RA molecule replaced into the CyDs cavity. Moreover, the RDF plots for O1, O2, O7, and O8 atoms, H2, H3, H13 and H15 (phenolic O and H), O3, O4 and H14 (acidic H and O), O5 and O6 (ester O) of RA molecules concerning β-CyD: RA IC and γ-CyD: RA IC is plotted in Fig. 12-c, and Fig. ESI 5-c, respectively. As illustrated in Fig. 12-c, the RDF plots of H atoms are in the range of 1.5 to 2.3 Å with the maximum value of g(r) ≈ 2.68 for H14 atom (acidic hydrogen) of 2.68. it can be concluded that this H has the highest number of hydrogen bonds with water molecules and is available to water molecules. Also, in the following classes, the decreases in g(r) were H13, H2, H3, and H15. The O atoms, in the range of 2.4 to 3.4 Å with g(r) ≈ 1.38 for O1 (C3'-phenolic) and the other O's indicated lower in g (r) and lower in intensity, respectively. In the RA molecule in γ-CyD: RA IC, the RDF plots of H atoms are in the range of 1.5 to 2.3 Å. because of the highest number of hydrogen bonding with water molecules, the H14 atom (acidic hydrogen) has been indicated the maximum value of g(r) ≈ 2.25. Moreover, the H13, H2, H3, and H15 are showed lower values of g(r), respectively. The O atoms, in the range of 2.4 to 3.4 Å, the highest value g(r) ≈ 1.47 has been shown for the O1 (C3'-phenolic), and the other O's indicated lower in g (r) and intensity, respectively. Because the esterified (O5) of the RA molecule is introduced into the cavities of β- and γ-CyDs, so it could not form a specific hydrogen bond with the water molecules, so the RDF peak did not show (See Fig. ESI 5-c).

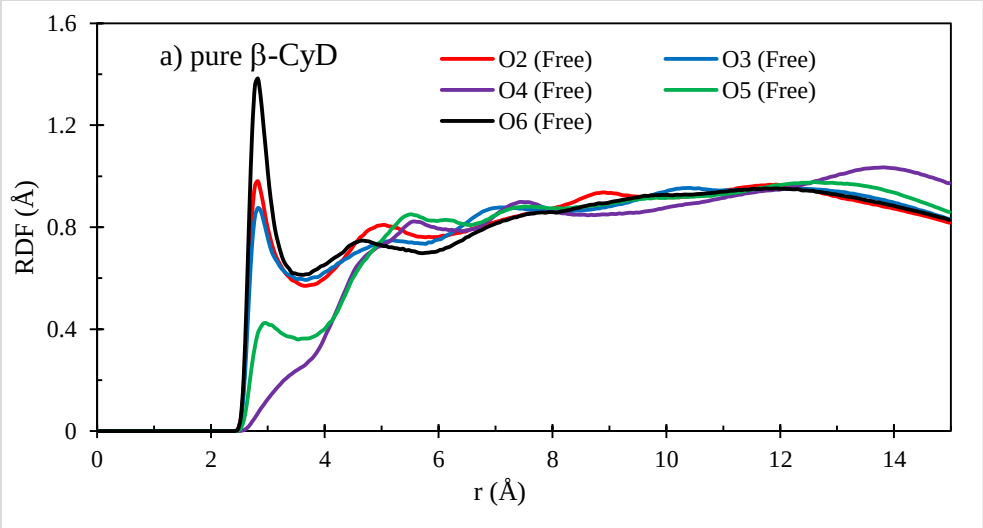
a) pure β-CyD
O2 (Free)
O3 (Free)
O4 (Free)
O5 (Free)
O6 (Free)
RDF (Å)
r (Å)

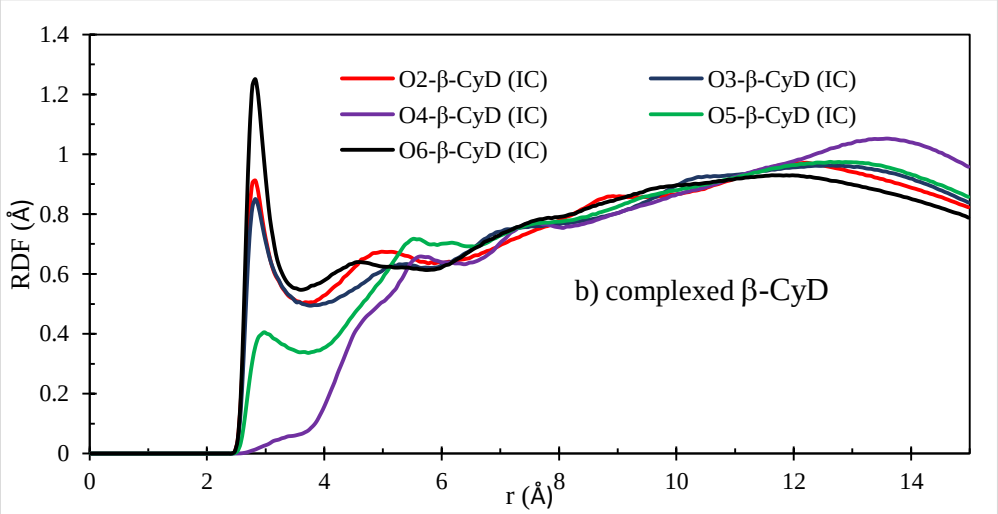
O2-β-CyD (IC)
O3-β-CyD (IC)
O4-β-CyD (IC)
O5-β-CyD (IC)
O6-β-CyD (IC)
b) complexed β-CyD
RDF (Å)
r (Å)

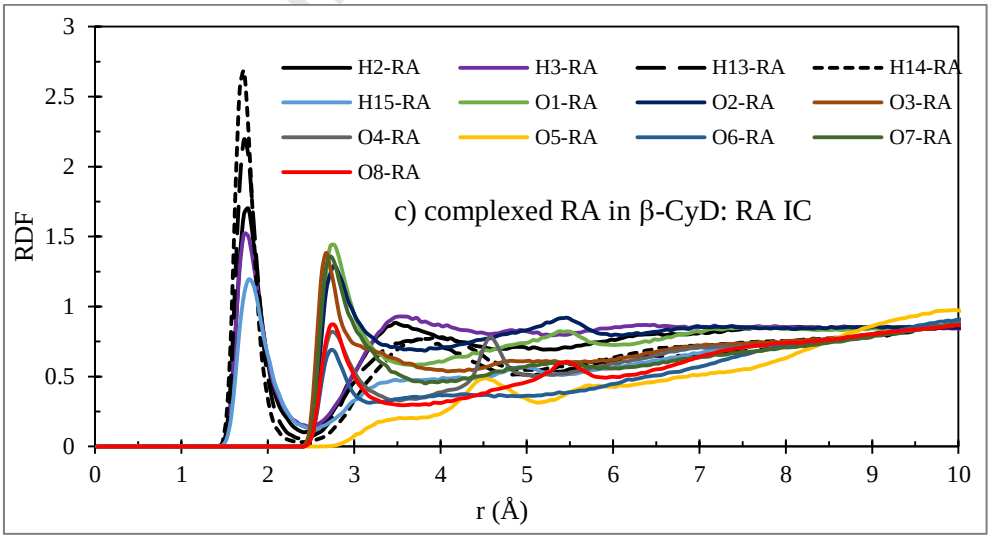
H2-RA
H3-RA
H13-RA
H14-RA
H15-RA
O1-RA
O2-RA
O3-RA
O4-RA
O5-RA
O6-RA
O7-RA
O8-RA
c) complexed RA in β-CyD: RA IC
RDF
r (Å)

Fig. 12): RDF of waters around the oxygen atoms O2, O3, O4, O5 and O6 for a) pure β-CyD, b) β-CyD: RA IC, and also the oxygens and hydrogen atoms O1, O2, O7, and O8 atoms, H2, H3, H13 and H15 (phenolic O and H), O3, O4 and H14 (acidic H and O), O5 and O6 (ester O) of RA molecule in c) β-CyD: RA IC during 50 ns simulation data.

A solvent-accessible surface area (SASA) is the area on the surface of the biomacromolecules such as CyDs can be in contact with solvents [47,48]. SASA is calculated for β- and γ-CyD in the pure and complexed states with RA during 50 ns MD simulation and is shown in Fig. 13.
As presented in Table 6, lower values of SASA for the IC in comparison to free CyDs could be related to the essential role of van der Waals interactions in the IC formations, water release, and insertion of RA into the cavity of CyDs. The Buried surface area (BSA), is the part of the macromolecular surface that is coated during the complex formation. As shown in Fig. 13 and Table 6, the BSA is this difference between the SASA in complex state and free state. See the following equation:

$$BSA(\text{Å}^2) = SASA(free) - SASA(IC) \qquad (9)$$

The RDF diagrams (Fig. 12 and Fig. ESI 5) also confirmed lower SASA for the ICs than pure CyDs.

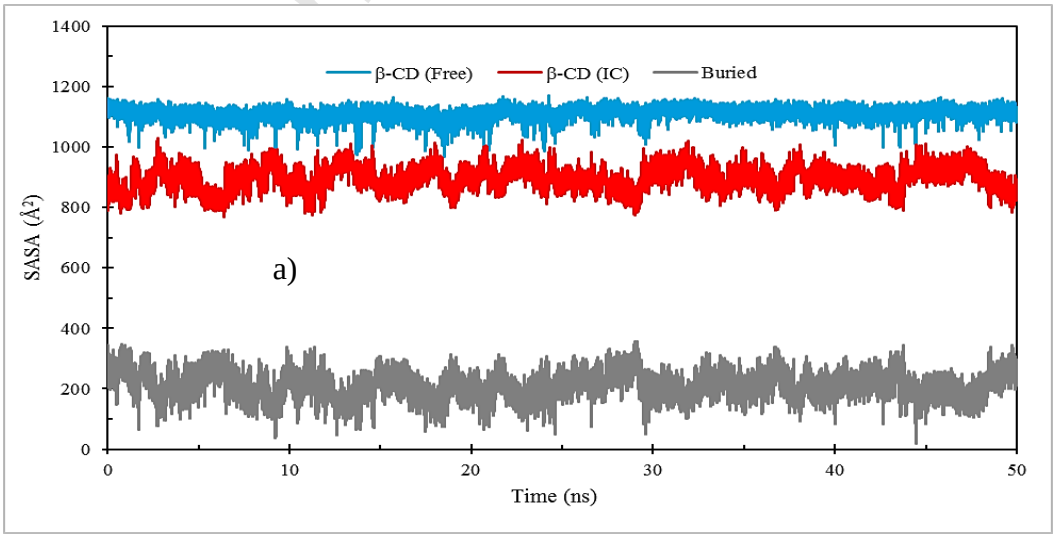

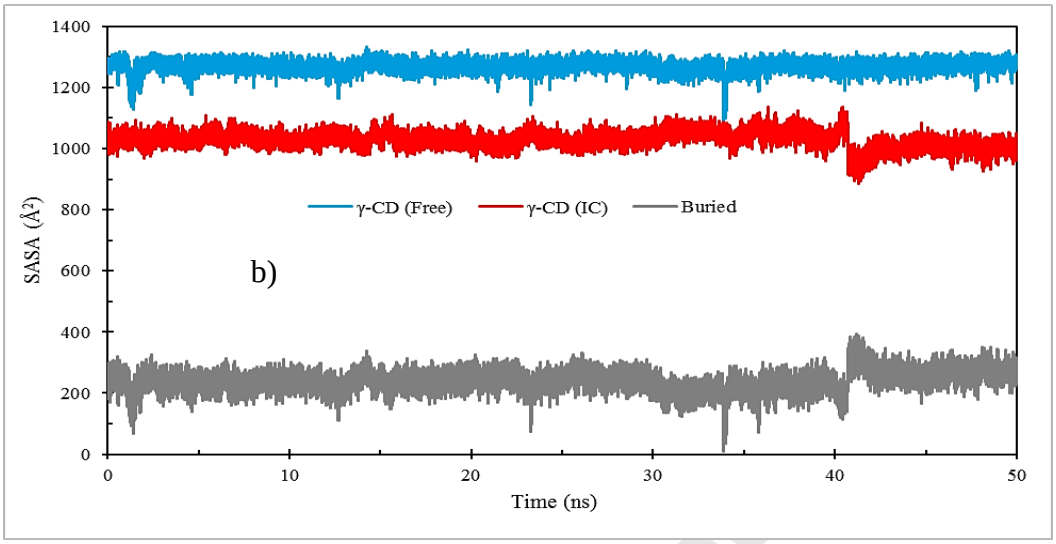

Fig. 13): SASA (Å^2) in the absence and presence of RA and BSA (Å^2) for a) β-CyD and b) γ-CyD during 50 ns simulation time.

Table 6): SASA (Å^2) for β- and γ-CyD in the absence and presence of RA and BSA (Å^2) with RA during 50 ns simulation time.

CyDs	SASA (Å^2) for Free	SASA (Å^2) for IC	BSA (Å^2)
β-CyD	1107.800 ± 20.124	954.269 ± 20.501	153.576 ± 27.586
γ-CyD	1267.867 ± 19.047	1024.400 ± 25.827	240.421 ± 33.303

The structural stability of CyDs: Drug IC have been investigated through the analysis of intermolecular hydrogen bonding. The angle and distance between the donor and acceptor of a hydrogen bond should be > 30° and >0.35 nm, respectively, that 0.35 nm value is related to the first hydration shell with the molecules of water (See RDF plot) [49]. The module of the CPPTRAJ estimated the formation of hydrogen bond numbers between molecules of β- and γ-CyDs (Scheme 1a), and RA (Scheme 1b) at the 50 ns simulation time. In Table 7 was summarized the results of the analysis of hydrogen bonds between β- and γ-CyDs with RA. As observed in Table 7-a, several hydrogen bonds were formed between O and H atoms of the RA molecules with the O2, O3, O4, and O6 atoms of the β-CyD molecule. These consequences were conforming to the molecular docking analysis, spectroscopies of ^{1}H-NMR, and ICD and indicating the location of RA (A-ring) in the broader side of the β-CyD cavity and B-ring of RA

in the narrower side of β-CyD. Furthermore, the kind and hydrogen bond numbers between γ-CyD and RA have been shown in Table 7-b. Some of the hydrogen bonds were formed between H and O atoms of RA molecules with O2, O3, O4 and O6 atoms of the γ-CyD. The results indicated that the folding of the RA compound and the locating of the A and B rings of the RA compound were close the narrower side of γ-CyD and the proximity of the carboxylic group (C9') of the RA compound in the broader side of this CyD. The results of hydrogen bonding analysis could be confirmed by ^{1}H-NMR, molecular docking, and ICD spectroscopy for the encapsulation of RA by γ-CyD.

Table 7: The occupations of hydrogen bonds numbers for a) β-CyD and b) with RA during the 50 ns simulation time.

The hydrogen bonding interaction kind	intermolecular Hydrogen bonding Number
a) β-CyD: RA IC	
H-O (C3'-A ring)… H-O^{2}	192
H-O (C3'-A ring)… H-O^{3}	276
H-O (C4'-A ring)… H-O^{2}	75
H-O (C4'-A ring)… H-O^{3}	123
H-O (C3-B ring)… H-O^{6}	1308
H-O (C4-B ring)… H-O^{6}	497
H-O (C9')… H-O^{2}	59
H-O (C9')… H-O^{3}	52
b) γ-CyD: RA IC	
H-O (C3'-A ring)… H-O^{2}	80
H-O (C3'-A ring)… H-O^{3}	59
H-O (C3'-A ring)… H-O^{6}	608
H-O (C4'-A ring)… H-O^{2}	26
H-O (C4'-A ring)… H-O^{6}	44
H-O (C3-B ring)… H-O^{6}	16
H-O (C4-B ring)… H-O^{6}	7
H-O (C9')… H-O^{2}	6
H-O (C9')… H-O^{3}	20

H-O (C9')… H-O[6]	4

The thermodynamic parameters for β- and γ-CyDs: RA ICs have been computed thorough MM-PBSA/GBSA techniques at 50 ns simulation time and listed in Tables 8. The energetic components are included of the gas phase energy (ΔG_{gas}) achieved via the summation between electrostatic (ΔE_{ele}) and van der Waals (ΔE_{vdw}) energies, the free energy of solvation (ΔG_{solv}) and entropy contribution ($T\Delta S$). These results determined the facility to calculate the relative free binding energies ($\Delta G_{MM\text{-}PBSA}$ and $\Delta G_{MM\text{-}GBSA}$) for complexation RA with β- and γ-CyDs. The intermolecular van der Waals interaction (ΔE_{VDW}) obtained the critical contribution to the insertion of RA into the β- and γ-CyD cavities. The formation and stability of ICs were studied by experimental methods, for instance, thermodynamics parameters analysis by phase solubility diagram and suggested that the IC formation between β- and γ-CyDs and RA lead to exothermic and enthalpy-driven ($\Delta H < 0$) in nature. These consequences are inconsistent with the MM-PBSA/GBSA methods. The ΔE_{VDW} contribution for these ICs was more substantial than ΔE_{ele} contribution. Subsequently, the results point to the intermolecular van der Waals interactions to the total interaction energy than any other type of interaction. It should be noted that the results of the study of these two types of ICs are similar [50–52].

Table 8: Energetic analysis for a) β-CyD: RA IC and b) γ-CyD: RA IC by the MM-PBSA/GBPBSA solvation models during 50 ns MD simulation.

a) β-CyD: RA IC			
ΔE_{ele}	-2.59 ± 1.70	ΔE_{ele}	-2.59 ± 1.70
ΔE_{VDW}	-35.36 ± 2.25	ΔE_{VDW}	-35.36 ± 2.25
ΔG_{gas}*	-37.95 ± 3.22	ΔG_{gas}*	-37.95 ± 3.22
ΔG_{solv}*	26.86 ± 1.49	ΔG_{solv}*	8.04 ± 1.62
$\Delta G_{MM\text{-}PBSA}$*	-11.82 ± 2.77	$\Delta G_{MM\text{-}GBSA}$*	-29.91 ± 2.22
$T\Delta S$**	-20.64 ± 0.66	$T\Delta S$**	-20.64 ± 0.66
ΔH*	-32.46 ± 2.85	ΔH*	-50.55 ± 2.31
b) γ-CyD: RA IC			
ΔE_{ele}	-2.90 ± 1.30	ΔE_{ele}	-2.90 ± 1.30
ΔE_{VDW}	-36.91 ± 1.93	ΔE_{VDW}	-36.91 ± 1.93
ΔG_{gas}*	-39.80 ± 2.55	ΔG_{gas}*	-39.80 ± 2.55
ΔG_{solv}*	28.24 ± 1.49	ΔG_{solv}*	7.95 ± 1.31
$\Delta G_{MM\text{-}PBSA}$*	-11.56 ± 2.54	$\Delta G_{MM\text{-}GBSA}$*	-31.85 ± 1.84
$T\Delta S$**	-20.62 ± 0.67	$T\Delta S$**	-20.62 ± 0.67
ΔH*	-32.18 ± 2.63	ΔH*	-52.47 ± 1.96

* *ΔH and ΔG:* kcal mol^{-1}

** *TΔS*: kcal mol^{-1}

Conclusions

In this research, the formulation of RA as an antioxidant and anti-inflammatory compound with β- and γ-CyD as the nano-cavities with 1:1 stoichiometry (A_L type) were prepared and characterized comprehensively with various experimental and computational methods. Our conclusions indicate that the formation of β- and γ-CyDs: RA ICs are the exothermic process with the enthalpy-driven mechanism and the most prominent role of hydrogen bonding and hydrophobic interactions in the complexation process. The encapsulation RA into the cavities of

β- and γ-CyDs led to the formation of the water-soluble and photo-stable ICs. The ^{1}H-NMR analysis and the molecular docking calculation indicated that the RA was found in the vicinity of the broader and narrower rims of β-CyD and case of γ-CyD: RA IC, the A and B rings of RA were close the narrower side of γ-CyD and the proximity of the carboxylic group (C9') of the RA compound in the broader side of this CyD. Also, these results are confirmed by ^{1}H-NMR and ICD spectroscopic methods.

Additionally, these experimental results are confirmed by the molecular docking and MD simulations via various parameters, i.e., snapshot analysis, RMSD, RMSF, RDF, H-bond, SASA, and distance and also the MM-PBSA and MM-GBSA implicit solvation models. These results indicated that among the natural cyclodextrins, β- and γ-CyDs as the best choice for the encapsulation of RA. These two CyD could be used in the solubility, stability and bioavailability, enhancement of RA in encapsulation with them. As well between two CyDs, the β-CyD: RA IC is more stable than γ-CyDs: RA IC, therefore, β-CD is the best choice for encapsulation of RA among the other natural CyDs. Overall, this investigation may provide the possibility for biomedical applications of food industries, represent the antioxidant activity conservation, anticancer, and anti-inflammatory.

Acknowledgments

The authors gratefully acknowledge the Research Council of the University of Isfahan and Institute of Biochemistry and Biophysics (IBB) of the University of Tehran (UT) for financial supports.

References:

[1] R. Tsao, Chemistry and Biochemistry of Dietary Polyphenols, Nutrients. 2 (2010) 1231–1246.

[2] H. El Gharras, Original Article Polyphenols: Food sources, Properties and Applications–A Review, Int. J. Food Sci. Technol. 44 (2009) 2512–2518.

[3] S.E. Çelik, M. Özyürek, A.N. Tufan, K. Güçü, R. Apak, N. Tufan, K. Güc, Spectroscopic Study and Antioxidant Properties of the Inclusion Complexes of Rosmarinic acid with Natural and Derivative Cyclodextrins, Spectrochim. Acta - Part A Mol. Biomol. Spectrosc. 78 (2011) 1615–1624.

[4] K. Shetty, Biosynthesis and Medical Applications of Rosmarinic Acid, J. Herbs. Spices Med. Plants. (2001) 161–181.

[5] M. Alagawany, M.E.A. El-hack, M.R. Farag, M. Gopi, K. Karthik, Y.S. Malik, K. Dhama, Rosmarinic acid : Modes of action, Medicinal Values and Health Benefits, Anim. Heal. Res. Rev. 18 (2017) 167–176.

[6] M. Ari, Ä.D.E.L.B. An, J.U.A.N.L. Orente, J. Ulia, O.B.B.E. Arci, Phenolic Diterpenes, Flavones, and Rosmarinic Acid Distribution during the Development of Leaves, Flowers, Stems, and Roots of Rosmarinus officinalis. Antioxidant Activity, J. Agric. Food Chem. 51 (2003) 4247–4253.

[7] T. Friedman, The Effect of Rosmarinic Acid on Immunological and Neurological Systems: A Basic Science and Clinical Review, J. Restor. Med. 4 (2015) 50–59.

[8] B. Medronho, A. J. M. Valente, P. Costa, A. Romano, Inclusion Complexes of Rosmarinic acid and Cyclodextrins: Stoichiometry, association Constants, and Antioxidant Potential, Colloid Polym. Sci. 292 (2014) 885–894.

[9] F. Zhu, T. Asada, A. Sato, Y. Koi, H. Nishiwaki, H. Tamura, Rosmarinic Acid Extract for Antioxidant, Antiallergic, and α - Glucosidase Inhibitory Activities, Isolated by Supramolecular Technique and Solvent Extraction from Perilla Leaves, Aggricultural Food Chem. 62 (2014) 885–892.

[10] A. Aksamija, A. Polidori, R. Plasson, O. Dangles, V. Tomao, The Inclusion Complex of Rosmarinic acid into beta-Cyclodextrin: A Thermodynamic and Structural Analysis by NMR and Capillary Electrophoresis, Food Chem. 208 (2016) 258–263.

[11] E.M.M. Del Valle, Cyclodextrins and their Uses: A Review, Process Biochem. 39 (2004) 1033–1046.

[12] T. Loftsson, D. Duchêne, Cyclodextrins and their Pharmaceutical Applications, Int. J. Pharm. 329 (2007) 1–11.

[13] U.R. Bhaskara-Amrit, P.B. Agrawal, M.M.C.G. Warmoeskerken, Applications of β-Cyclodextrins in Textiles, Autex Res. J. 11 (2011) 94–101.

[14] L. Szente, J. Szejtli, Cyclodextrins as Food Ingredients, Trends Food Sci. Technol. 15 (2004) 137–142.

[15] I. Zarandona, C. Barba, P. Guerrero, K. de la Caba, J. Maté, Development of Chitosan films Containing β-cyclodextrin Inclusion Complex for Controlled Release of Bioactives, Food Hydrocoll. 104 (2020).

[16] Z. Li, M. Wang, F. Wang, Z. Gu, G. Du, J. Wu, J. Chen, γ-Cyclodextrin: A Review on Enzymatic Production and Applications, Appl. Microbiol. Biotechnol. 77 (2007) 245–255.

[17] Z. Xiao, W. Hou, Y. Kang, Y. Niu, X. Kou, Encapsulation and Sustained Release Properties of Watermelon Flavor and its Characteristic Aroma Compounds from γ-cyclodextrin Inclusion Complexes, Food Hydrocoll. 97 (2019).

[18] G. Crini, Review: A History of Cyclodextrins, Chem. Rev. 114 (2014) 10940–10975.

[19] G. Astray, C. Gonzalez-Barreiro, J.C. Mejuto, R. Rial-Otero, J. Simal-Gándara, A review on the use of cyclodextrins in foods, Food Hydrocoll. 23 (2009) 1631–1640.

[20] J.M. López-Nicolás, P. Rodríguez-Bonilla, F. García-Carmona, Cyclodextrins and Antioxidants, Crit. Rev. Food Sci. Nutr. 54 (2012) 251–276.

[21] F. Fateminasab, A.K. Bordbar, S. Shityakov, S. Gholami, Diadzein Complexation with Unmodified Cyclodextrins: A Detailed Experimental and Theoretical Study, J. Mol. Liq. 271 (2018) 80–95.

[22] F. Fateminasab, A.K. Bordbar, S. Shityakov, Detailed chemical characterization and molecular modeling of serotonin inclusion complex with unmodified β-cyclodextrin, Heliyon. 5 (2019) 1–30.

[23] T. Higuchi, K.A. Connors, Phase-Solubility Techniques, Adv. Anal. Chem. Instrum. 4 (1965) 212–217.

[24] C.K.A. Higuchi T, Phase solubility diagram, Adv. Anal. Chem. Instrum. 4 (1965) 117–212.

[25] J. Rakmai, B. Cheirsilp, J.C. Mejuto, A. Torrado-Agrasar, J. Simal-Gándara, Physico-chemical Characterization and Evaluation of Bio-efficacies of Black Pepper Essential Oil Encapsulated in Hydroxypropyl-beta-cyclodextrin, Food Hydrocoll. 65 (2017) 157–164.

[26] D. Papachristodoulou, A. Snape, W.H. Elliott, Energy Considerations in Biochemistry, in: Biochem. Mol. Biol., Oxford University Press, united kingdom, 2014: p. 30.

[27] M. Kfoury, L. Auezova, H. Greige-Gerges, S. Ruellan, S. Fourmentin, Cyclodextrin, an Efficient Tool for Trans-anethole Encapsulation: Chromatographic, Spectroscopic, Thermal and Structural Studies, Food Chem. 164 (2014) 454–461.

[28] R. Ragno, A. Tramontano, A. Martinelli, T. Tuccinardi, Molecular Docking Tutorial, VI Eur. Work. Drug Des. (2007) 48.

[29] J. Wang, R.M. Wolf, J.W. Caldwell, P.A. Kollman, D.A. Case, Development and Testing of a General Amber Force Field, J. Comput. Chem. 25 (2004) 1157–1174.

[30] C. Cézard, X. Trivelli, F. Aubry, F. Djedaïni-Pilard, F.-Y.Y. Dupradeau, Molecular Dynamics Dtudies of Native and Substituted Cyclodextrins in Different Media: 1. Charge Derivation and Force Field Performances., Phys. Chem. Chem. Phys. 13 (2011) 15103–15121.

[31] P. Mark, L. Nilsson, Structure and Dynamics of the TIP3P, SPC, and SPC/E Water Models at 298 K, J. Phys. Chem. A. 105 (2001) 9954–9960.

[32] C. Wang, D.A. Greene, L. Xiao, R. Qi, R. Luo, R. Luo, Recent Developments and Applications of the MMPBSA Method, Front. Mol. Biosci. 4 (2018) 1–18.

[33] I. Mourtzinos, N. Kalogeropoulos, S.E. Papadakis, K. Konstantinou, V.T. Karathanos, Encapsulation of Nutraceutical Monoterpenes in β-Cyclodextrin and Modified Starch, J. Food Sci. 73 (2008) 89–94.

[34] N. Roik, L. Belyakova, IR Spectroscopy, X-ray Diffraction and Thermal Analysis studies of Solid "β-Cyclodextrin-para-Aminobenzoic Acid" Inclusion Complex, Phys. Chem. Solid State. 1 (2011) 168–173.

[35] R. Zhao, C. Sandström, H. Zhang, T. Tan, NMR Study on the Inclusion Complexes of β-Cyclodextrin with Isoflavones., Molecules. 21 (2016) 1–11.

[36] Y. Wu, Y. Xiao, Y. Yue, K. Zhong, Y. Zhao, H. Gao, A Deep Insight into Mechanism for Inclusion of 2R,3R-Dihydromyricetin with Cyclodextrins and the Effect of Complexation on Antioxidant and Lipid-Lowering Activities, Food Hydrocoll. 103 (2020) 1–9.

[37] M. Quilaqueo, S. Millao, I. Luzardo-Ocampo, R. Campos-Vega, F. Acevedo, C. Shene, M. Rubilar, Inclusion of Piperine in β-Cyclodextrin Complexes Improves their Bioaccessibility and in Vitro Antioxidant Capacity, Food Hydrocoll. 91 (2019) 143–152.

[38] K. Harata, H. Uedaira, The Circular Dichroism Spectra of the β-Cyclodextrin Complex with Naphthalene Derivatives, Bull. Chem. Soc. Jpn. 48 (1975) 375–378.

[39] A.D. Bani-Yaseen, N.F. Al-Rawashdeh, I. Al-Momani, Influence of Inclusion complexation with β-cyclodextrin on the Photostability of Selected Imidazoline-derived Drugs, J. Incl. Phenom. Macrocycl. Chem. 63 (2009) 109–115.

[40] R. Amorati, L. Valgimigli, Modulation of the Antioxidant Activity of Phenols by Non-Covalent Interactions, Org. Biomol. Chem. 10 (2012) 4147–4158.

[41] M.J.T.J. Arts, G.R.M.M. Haenen, L.C. Wilms, S.A.J.N. Beetstra, C.G.M. Heijnen, H.P. Voss, A. Bast, Interactions between Flavonoids and Proteins: Effect on the Total Antioxidant Capacity, J. Agric. Food Chem. 50 (2002) 1184–1187.

[42] A. Munin, F. Edwards-lévy, Encapsulation of Natural Polyphenolic Compounds; A Review, Pharmaceutics. 3 (2011) 793–829.

[43] S. Shityakov, J. Broscheit, C. Förster, α-Cyclodextrin Dimer Complexes of Dopamine and Levodopa Derivatives to Assess Drug Delivery to the Central Nervous System: ADME and Molecular docking Studies, Int. J. Nanomedicine. 7 (2012) 3211–3219.

[44] D.R. Roe, T.E. Cheatham III, PTRAJ and CPPTRAJ: Software for Processing and Analysis of Molecular Synamics Trajectory data, J Chem Theory Com. 9 (2013) 3084–3095.

[45] W. Cai, T. Sun, C. Chipot, Can the Anomalous Aqueous Solubility of β-Cyclodextrin be Explained by its Hydration Free Energy Alone?, Phys. Chem. Chem. Phys. 10 (2008) 3236–3243.

[46] M. Jana, S. Bandyopadhyay, Molecular Dynamics Study of β-Cyclodextrin-Phenylalanine (1:1) Inclusion Complex in Aqueous Medium, J. Phys. Chem. B. 117 (2013) 9280–9287.

[47] B. Lee, F.M. Richards, The Interpretation of Protein Structures: Estimation of Static Accessibility, J. Mol. Biol. 55 (1971) 379–400.

[48] E. Durham, B. Dorr, N. Woetzel, R. Staritzbichler, J. Meiler, Solvent Accessible Surface Area Approximations for Rapid and Accurate Protein Structure Prediction, J. Mol. Model. 15 (2009) 1093–1108.

[49] W. Khuntawee, P. Wolschann, T. Rungrotmongkol, J. Wong-Ekkabut, S. Hannongbua, Molecular Dynamics Simulations of the Interaction of Beta Cyclodextrin with Lipid Bilayer, J. Chem. Inf. Model. 55 (2015) 1894-1902.

[50] J.E.H. Köhler, N. Grczelschak-mick, J. Erika, The β-Cyclodextrin/Benzene Complex and its Hydrogen Bonds– A Theoretical Study Using Molecular Dynamics, Quantum Mechanics and COSMO-RS, Beilstein J. Org. Chem. 9 (2013) 118–134.

[51] E. Sarukhanyan, S. Shityakov, T. Dandekar, Rational Drug Design of Axl Tyrosine Kinase Type I Inhibitors as Promising Candidates Against Cancer, Front. Chem. 7 (2020) 1–40.

[52] T. Hou, J. Wang, Y. Li, W. Wang, Assessing the Performance of the MM_PBSA and MM_GBSA Methods. 1. The Accuracy.pdf, J. Chem. Inf. Model. 51 (2011) 69–82.

Author statement

The following authors have contributed to the manuscript:

Fatemeh Fateminasab: As a Ph.D. student, she designed methodology and obtain data, theoretically and experimentally. She also did data analysis and wrote the first draft of the manuscript.

Abdol-Khalegh Bordbar: As the second supervisor, he guided methodology and data analysis. He edited and modified the manuscript.

Sergey Shityakov: As the advisor, he controlled the using the software methodology and obtain data theoretically. He gave useful comments to modify the first draft of the manuscript.

Ali Akbar Saboury: As the first supervisor, he controlled all methods and data analysis during the Ph.D. process. He edits and modified the manuscript from the first draft to the first revision.

We have no conflicts of interest.

Conflicts of Interest

Manuscript title: Molecular insights into inclusion complex formation between β- and γ-cyclodextrins and rosmarinic acid

The authors whose names are listed immediately below certify that they have NO affiliations with or involvement in any organization or entity with any financial interest (such as honoraria; educational grants; participation in speakers' bureaus; membership, employment, consultancies, stock ownership, or other equity interest; and expert testimony or patent-licensing arrangements), or non-financial interest (such as personal or professional relationships, affiliations, knowledge or beliefs) in the subject matter or materials discussed in this manuscript.

Author names:

1- Dr. Fatemeh Fateminasab (Department of Chemistry, University of Isfahan, Isfahan, 8174673441, Iran Email: ftmfatemi61@gmail.com Tel: +98-31-37935034)

2- Professor Abdol-Khalegh Bordbar (Department of Chemistry, University of Isfahan, Isfahan, 8174673441, Iran Email: akbordbar@gmail.com or bordbar@chem.ui.ac.ir Tel: +98-31-37934941 Fax: +98-31-3668973)

3- Dr. Sergey Shityakov (Department of Bioinformatics, University of Würzburg, 97074, Würzburg, Germany Email: shityakoff@hotmail.com Tel.: +49-931-2013-0016; Fax: +49-931-2013-0019)

4- Professor Ali Akbar Saboury (Institute of Biochemistry and Biophysics, University of Tehran, Tehran Email: saboury@ut.ac.ir, Tel: +98-21-66956984).

The authors whose names are listed immediately below report the following details of affiliation or involvement in an organization or entity with a financial or non-financial interest in the subject matter or materials discussed in this manuscript. Please specify the nature of the conflict on a separate sheet of paper if the space below is inadequate.

Author names:

Author's name (typed)	Author's signature	Date
1- Fatemeh Fateminasab	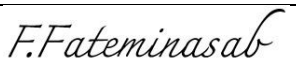	29 June 2020
2- Abdol-Khalegh Bordbar	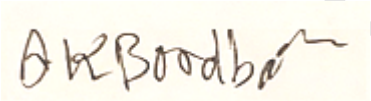	29 June 2020
3- Sergey Shityakov		29 June 2020
4- Ali Akbar Saboury		29 June 2020

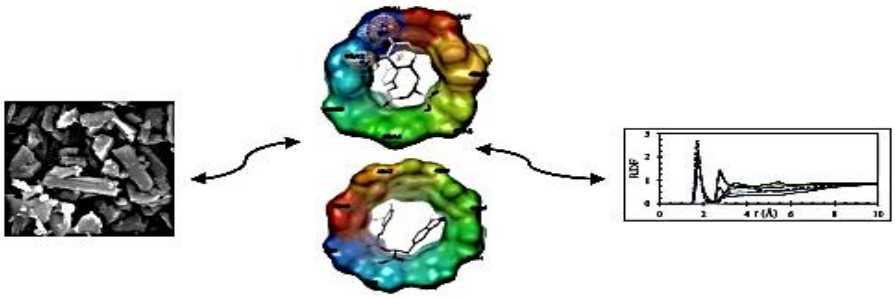

Graphical abstract

Highlights

1- The β- & γ-β-CyD: RA ICs show A_L type solubility and 1:1 stoichiometry.
2- The improvement of solubility and photo-stability were observed for these ICs.
3- The computational methods represent the insertion of RA into the CyD cavities.
4- These ICs can be used in food industries due to their antioxidant properties.